

WEAKLY IMPLICIT NUMERICAL SCHEMES FOR A TWO-FLUID MODEL*

STEINAR EVJE[†] AND TORE FLÄTTEN[‡]

Abstract. The aim of this paper is to construct semi-implicit numerical schemes for a two-phase (two-fluid) flow model, allowing for violation of the CFL criterion for sonic waves while maintaining a high level of accuracy and stability on volume fraction waves.

By using an appropriate hybridization of a robust implicit flux and an upwind explicit flux, we obtain a class of first-order schemes, which we refer to as *weakly implicit mixture flux* (WIMF) methods. In particular, by using an advection upstream splitting method (AUSMD) type of upwind flux [S. Evje and T. Flåtten, *J. Comput. Phys.*, 192 (2003), pp. 175–210], we obtain a scheme denoted as WIMF-AUSMD.

We present several numerical simulations, all of them indicating that the CFL-stability of the WIMF-AUSMD scheme is governed by the velocity of the volume fraction waves and not the rapid sonic waves. Comparisons with an explicit Roe scheme indicate that the scheme presented in this paper is highly efficient, robust, and accurate on slow transients. By exploiting the possibility to take much larger time steps, it outperforms the Roe scheme in the resolution of the volume fraction wave for the classical water faucet problem. On the other hand, it is more diffusive on pressure waves.

Although conservation of positivity for the masses is not proved, we demonstrate that a fix may be applied, making the scheme able to handle the transition to one-phase flow while maintaining a high level of accuracy on volume fraction fronts.

Key words. two-phase flow, two-fluid model, hyperbolic system of conservation laws, flux splitting, implicit scheme

AMS subject classifications. 76T10, 76N10, 65M12, 35L65

DOI. 10.1137/030600631

1. Introduction. This paper deals with numerical solutions to a classical four-equation *two-fluid* model for isentropic flows in one space dimension. The model we will be concerned with (described in detail in section 2) is classified as a hyperbolic set of differential equations, with the implication that information flows in the system along characteristic curves with a certain velocity. For such models *explicit* numerical schemes are commonly used, advantage being taken of the fact that the time development of the state at some point depends only on points within the span of the characteristic curves in time and space. Explicit schemes are simple to implement and may give more flexibility in the treatment of complex pipe networks. However, they are subject to the CFL constraint

$$(1) \quad \frac{\Delta x}{\Delta t} \geq |\lambda_{\max}|,$$

where λ_{\max} is the largest eigenvalue for the system. For the two-fluid model we are concerned with, the four eigenvalues are pairwise associated with sonic and volume fraction waves [9]. The sonic waves may be several orders of magnitude faster than the volume fraction waves, although the latter may often be of greater interest to the

*Received by the editors August 7, 2003; accepted for publication (in revised form) July 8, 2004; published electronically April 19, 2005.

<http://www.siam.org/journals/sisc/26-5/60063.html>

[†]RF-Rogaland Research, Prof. Olav Hanssensvei 15, Stavanger, Norway (steinar.evje@rf.no).

[‡]Department of Energy and Process Engineering, Norwegian University of Science and Technology, Kolbjørn Hejes vei 1B, N-7491, Trondheim, Norway (tore.flatten@maskin.ntnu.no). This author was supported in part by the Petronics program of the Norwegian Research Council.

researcher. For this reason the CFL criterion (1) may severely limit the computational efficiency of explicit schemes.

To remedy the situation, a step in a more implicit direction, i.e., coupling one or more variables throughout the computational domain, may be made. Such approaches may be classified as follows:

- *Weakly implicit.* The original CFL criterion (1) may be broken for sonic waves, but a weaker CFL criterion for volume fraction waves still applies,

$$(2) \quad \frac{\Delta x}{\Delta t} \geq |\lambda_{\max}^v|,$$

where λ_{\max}^v is the largest of the two eigenvalues corresponding to volume fraction waves.

- *Strongly implicit.* No CFL-like stability criterion applies and the equations may be integrated with arbitrary time step. However, stability could be affected by other issues, such as inherent stiffness of the equations.

Most engineering computer software for two-fluid simulations seem to be based on some implicit approach. Examples include the CATHARE code [2], developed for the nuclear industry, and OLGA [3], aimed toward the petroleum industry. The recently developed PeTra [12] is largely based on the OLGA approach, being strongly implicit in the sense of the classification above. Weakly implicit numerical schemes for two-phase flow models have been investigated by Faille and Heintzé [10] and Masella et al. [14].

In recent years there have been several new applications of different upwind techniques for the equations of two-phase flow. Examples include implementations of the Roe scheme by Toumi and Kumbaro [26], Toumi [25], Cortese, Debussche, and Toumi [5], Romate [21], and Fjelde and Karlsen [11]. Masella, Faille, and Gallouet [15] implemented a rough Godunov scheme. A different approach was undertaken by Coquel et al. [4], who studied kinetic upwind schemes for the approximation of a two-fluid model. Saurel and Abgrall studied a general compressible unconditionally hyperbolic two-phase model with a wide range of applications [22, 23].

For one-phase flow, Wada and Liou [28] suggested a hybrid flux difference splitting (FDS) and flux vector splitting (FVS) scheme with good accuracy and stability properties. Their idea was extended to two-phase flow models by Edwards, Franklin, and Liou [6], Niu [16, 17], and Evje and Fjelde [7, 8] and Evje and Flåtten [9].

The aim of this work is to develop a general methodology for constructing numerical schemes for the two-fluid model which possesses the following important properties:

- no use of Riemann solver or computation of nonlinear flux Jacobians;
- accurate and nonoscillatory resolution of mass fronts, i.e., slow-moving volume fraction waves, comparable with the resolution given by upwind type of schemes like the Roe scheme; and
- stability under the weak CFL condition (2).

To this aim, we introduce an approach which we denote as the mixture flux (MF) method, as it takes into account that the physical variables of the system (pressure and volume fractions) each depend on the simultaneous state of *both phases* when expressed in terms of conservative variables. In other words, they are properties of the two-phase mixture.

The MF method consists of the following basic steps:

- (a) derivation of a pressure evolution equation solved centrally at cell interfaces,
- (b) derivation of implicit numerical mass fluxes consistent with the pressure calculation (a), and

(c) hybridization of the implicit mass fluxes of (b) with upwind fluxes.

These steps are described in detail in sections 3 through 7. In particular, by using a hybridization of an *implicit* and an *explicit* flux in (c), we obtain what we denote as the *weakly implicit mixture flux* (WIMF) family of schemes. The WIMF approach allows us to unify two different aspects of two-phase flow calculation, namely, producing a high level of accuracy on volume fraction waves while allowing for violation of the sonic CFL criterion.

Our paper is organized as follows. In section 2 we present the two-fluid model we will be working with. In section 3 the MF approach is presented in a semidiscrete setting where the pressure evolution equation is introduced as well as the construction of mixture mass fluxes. These two steps constitute the main components of the MF methods. In section 4 we present a straightforward analysis demonstrating that the MF schemes possess some desirable properties relevant for their approximation properties.

Based on the semidiscrete scheme of section 3, we then in sections 5, 6, and 7 proceed to construct fully discrete first-order schemes which possess the properties identified in section 4. In section 8 we present numerical simulations where we attempt to shed light on the issues of stability, robustness, and accuracy for the scheme. We here also investigate how the scheme can handle a transition to one-phase flow using a transition fix similar to the one introduced in [9].

2. The two-fluid model. Throughout this paper we will be concerned with the common two-fluid model formulated by stating separate conservation equations for mass and momentum for the two fluids, which we will denote as a gas (g) and a liquid (l) phase. The model is identical to the model previously considered by Evje and Flåtten [9] and will be only briefly restated here. For a closer description of the terms and their significance, we refer to the previous work and the references therein.

2.1. Generally. We let \mathbf{U} be the vector of conserved variables,

$$(3) \quad \mathbf{U} = \begin{bmatrix} \rho_g \alpha_g \\ \rho_l \alpha_l \\ \rho_g \alpha_g v_g \\ \rho_l \alpha_l v_l \end{bmatrix} = \begin{bmatrix} m_g \\ m_l \\ I_g \\ I_l \end{bmatrix}.$$

By using the notation $\Delta p = p - p_i$, where p_i is the interfacial pressure, and $\tau_k = (p_i - p)\partial_x \alpha_k$, the model can be written in the form

- conservation of mass,

$$(4) \quad \frac{\partial}{\partial t} (\rho_g \alpha_g) + \frac{\partial}{\partial x} (\rho_g \alpha_g v_g) = 0,$$

$$(5) \quad \frac{\partial}{\partial t} (\rho_l \alpha_l) + \frac{\partial}{\partial x} (\rho_l \alpha_l v_l) = 0;$$

- conservation of momentum,

$$(6) \quad \frac{\partial}{\partial t} (\rho_g \alpha_g v_g) + \frac{\partial}{\partial x} (\rho_g \alpha_g v_g^2 + \alpha_g \Delta p) + \alpha_g \frac{\partial}{\partial x} (p - \Delta p) = Q_g + M_g^D,$$

$$(7) \quad \frac{\partial}{\partial t} (\rho_l \alpha_l v_l) + \frac{\partial}{\partial x} (\rho_l \alpha_l v_l^2 + \alpha_l \Delta p) + \alpha_l \frac{\partial}{\partial x} (p - \Delta p) = Q_l + M_l^D,$$

where for phase k the nomenclature is as follows:

- ρ_k —density,
- p —pressure,
- v_k —velocity,
- α_k —volume fraction,
- Δp —pressure correction at the gas-liquid interface,
- Q_k —momentum sources (due to gravity, friction, etc.), and
- M_k^D —interfacial drag force.

The volume fractions satisfy

$$(8) \quad \alpha_g + \alpha_l = 1.$$

For the numerical simulations presented in this work we assume the simplified thermodynamic relations

$$(9) \quad \rho_l = \rho_{l,0} + \frac{p - p_0}{a_l^2}$$

and

$$(10) \quad \rho_g = \frac{p}{a_g^2},$$

where

$$p_0 = 1 \text{ bar} = 10^5 \text{ Pa},$$

$$\rho_{l,0} = 1000 \text{ kg/m}^3,$$

$$a_g^2 = 10^5 (\text{m/s})^2,$$

and

$$a_l = 10^3 \text{ m/s}.$$

Moreover, we will treat Q_k as a pure source term, assuming that it does not contain any differential operators. We use the interface pressure correction

$$(11) \quad \Delta p = \Delta p(U, \delta) = \delta \frac{\alpha_g \alpha_l \rho_g \rho_l}{\rho_g \alpha_l + \rho_l \alpha_g} (v_g - v_l)^2,$$

where we set $\delta = 1.2$. This choice ensures that the model is a hyperbolic system of conservation laws; see, for instance, [26, 5]. Another feature of this model is that it possesses an approximate mixture sound velocity c given by

$$(12) \quad c = \sqrt{\frac{\rho_l \alpha_g + \rho_g \alpha_l}{\frac{\partial \rho_g}{\partial p} \rho_l \alpha_g + \frac{\partial \rho_l}{\partial p} \rho_g \alpha_l}}.$$

We refer to [26, 9] for more details.

Having solved for the conservative variable \mathbf{U} , we need to obtain the primitive variables (α_g, p, v_g, v_l) . For the pressure variable we see that by writing the volume fraction in equation (8) in terms of the conserved variables as

$$(13) \quad \frac{m_g}{\rho_g(p)} + \frac{m_l}{\rho_l(p)} = 1,$$

we obtain a relation yielding the pressure $p(m_g, m_l)$. Using the relatively simple equations of state (EOS) given by (9) and (10), we see that the pressure p is found as a positive root of a second-order polynomial. For more general EOS we must solve a nonlinear system of equations, for instance, by using a Newton–Raphson algorithm. Moreover, the fluid velocities v_g and v_l are obtained directly from the relations

$$v_g = \frac{U_3}{U_1}, \quad v_l = \frac{U_4}{U_2}.$$

Remark 1. Concerning the EOS for the liquid and gas phase, we would like to emphasize that the methods we develop do not require simple linear relations as given by (9) and (10). Formally, the only point of the algorithm which is affected by using more complicated EOS is the resolution algorithm which determines the pressure from the general relation (13).

2.2. Some useful differential relations. By differentiating the relation (13) we obtain the expressions

$$(14) \quad dp = \kappa(\rho_l dm_g + \rho_g dm_l)$$

and

$$(15) \quad d\alpha_l = \kappa \left(-\frac{\partial \rho_l}{\partial p} \alpha_l dm_g + \frac{\partial \rho_g}{\partial p} \alpha_g dm_l \right),$$

where

$$(16) \quad \kappa = \frac{1}{\frac{\partial \rho_l}{\partial p} \alpha_l \rho_g + \frac{\partial \rho_g}{\partial p} \alpha_g \rho_l}.$$

By combining (14) and (15) we can write the masses m_k in terms of a pressure and a volume fraction component as follows:

$$(17) \quad dm_g = \alpha_g \frac{\partial \rho_g}{\partial p} dp - \rho_g d\alpha_l$$

and

$$(18) \quad dm_l = \alpha_l \frac{\partial \rho_l}{\partial p} dp + \rho_l d\alpha_l.$$

The relations (14) and (15) reflect that differentials of the primitive variables α_l and p generally depend strongly on properties of the mixture of both masses through the differentials dm_g and dm_l . Later we will derive numerical mass fluxes which are consistent with the differential relations (14)–(18).

2.3. A pressure evolution equation. The relation (13) gives the pressure $p = p(m_g, m_l)$ through a state relation. Now we describe another procedure for determining the pressure through a dynamic relation.

Multiplying the gas mass conservation equation with $\kappa\rho_l$ and the liquid mass conservation equation with $\kappa\rho_g$ and adding the two resulting equations, we get

$$\kappa\rho_l \frac{\partial}{\partial t} m_g + \kappa\rho_g \frac{\partial}{\partial t} m_l + \kappa\rho_l \frac{\partial}{\partial x} (\rho_g \alpha_g v_g) + \kappa\rho_g \frac{\partial}{\partial x} (\rho_l \alpha_l v_l) = 0.$$

In view of (14) we get the nonconservative pressure evolution equation

$$(19) \quad \frac{\partial p}{\partial t} + \kappa \left(\rho_l \frac{\partial}{\partial x} (\rho_g \alpha_g v_g) + \rho_g \frac{\partial}{\partial x} (\rho_l \alpha_l v_l) \right) = 0,$$

where κ is given by (16). Coupling this pressure evolution equation to the momentum equations will be an important ingredient in allowing us to break the CFL criterion (2).

3. A semidiscrete scheme. In this section we construct semidiscrete approximations of solutions to (4)–(7). In sections 5, 6, and 7 we describe fully discrete approximations, and in section 8 we explore properties of these fully discrete schemes for several well-known two-phase flow problems.

3.1. General form. It will be convenient to express the model (4)–(7) on the following form:

$$(20) \quad \begin{aligned} \partial_t m_k + \partial_x f_k &= 0, \\ \partial_t I_k + \partial_x g_k + \alpha_k \partial_x p + (\Delta p) \partial_x \alpha_k &= Q_k, \end{aligned}$$

where $k = g, l$ and

$$\begin{aligned} f_k &= \rho_k \alpha_k v_k & \text{and} & & m_k &= \rho_k \alpha_k, \\ g_k &= \rho_k \alpha_k v_k^2 & \text{and} & & I_k &= \rho_k \alpha_k v_k. \end{aligned}$$

We assume that we have given approximations $(m_{k,j}^n, I_{k,j}^n) \approx (m_{k,j}(t^n), I_{k,j}(t^n))$. Approximations $m_{k,j}(t)$ and $I_{k,j}(t)$ for $t \in (t^n, t^{n+1}]$ are now constructed by solving the following ODE problem:

$$(21) \quad \begin{aligned} \dot{m}_{k,j} + \delta_x F_{k,j} &= 0, \\ \dot{I}_{k,j} + \delta_x G_{k,j} + \alpha_{k,j} \delta_x P_j + (\Delta p)_j \delta_x \Lambda_{k,j} &= Q_{k,j} \end{aligned}$$

subject to the initial conditions

$$m_{k,j}(t^n) = m_{k,j}^n, \quad I_{k,j}(t^n) = I_{k,j}^n.$$

Here δ_x is the operator defined by

$$\delta_x w_j = \frac{w_{j+1/2} - w_{j-1/2}}{\Delta x}, \quad \delta_x w_{j+1/2} = \frac{w_{j+1} - w_j}{\Delta x},$$

and $(\Delta p)_j(t) = (\Delta p)(U_j(t), \delta)$ is obtained from (11). Moreover, $F_{k,j+1/2}(t) = F_k(U_j(t), U_{j+1}(t))$, $G_{k,j+1/2}(t) = G_k(U_j(t), U_{j+1}(t))$, $P_{j+1/2}(t) = P(U_j(t), U_{j+1}(t))$,

and $\Lambda_{k,j+1/2}(t) = \Lambda_k(U_j(t), U_{j+1}(t))$ are assumed to be numerical fluxes consistent with the corresponding physical fluxes, i.e.,

$$\begin{aligned} F_k(U, U) &= f_k = \rho_k \alpha_k v_k, \\ G_k(U, U) &= g_k = \rho_k \alpha_k v_k^2, \\ P(U, U) &= p, \\ \Lambda_k(U, U) &= \alpha_k. \end{aligned}$$

The purpose now is to derive these numerical fluxes.

3.2. The numerical flux $\Lambda_{k,j+1/2}(t)$. We first start with the numerical flux $\Lambda_{k,j+1/2}(t)$. This term ensures that the system of equations becomes hyperbolic, but it is small in magnitude compared to other terms. Hence, for reasons of simplicity, we follow the approach of Paillère, Corre, and Cascales [18] and Coquel et al. [4] and discretize this term centrally. Thus we use the numerical flux

$$(22) \quad \Lambda_{k,j+1/2}(t) = \frac{\alpha_{k,j}(t) + \alpha_{k,j+1}(t)}{2}.$$

In the following we seek to discretize the remaining fluxes so that they are consistent with the underlying dynamics of the model. Essential information about the interplay between masses m_k and pressure p is given by the relation (13). We shall exploit this systematically when we devise numerical fluxes $F_{k,j+1/2}(t)$ and $P_{j+1/2}(t)$.

3.3. The numerical flux $P_{j+1/2}(t)$. To avoid an odd-even decoupling of the numerical pressure, we follow the approach of classical pressure-based schemes [19] in aiming to obtain an expression for $P_{j+1/2}$ involving a dynamical coupling to the cell center momentums. We hence suggest to associate the numerical flux $P_{j+1/2}(t)$ with the solution of the pressure evolution equation (19) and (16) discretized at the cell interface $j + 1/2$. More precisely, given the cell centered pressure $p_j^n \approx p(x_j, t^n)$ we determine $P_{j+1/2}(t)$ for $t \in [t^n, t^{n+1}]$ by solving the ODE

$$(23) \quad \begin{aligned} \dot{P}_{j+1/2} + [\kappa_{j+1/2} \rho_{1,j+1/2}] \delta_x I_{g,j+1/2} + [\kappa_{j+1/2} \rho_{g,j+1/2}] \delta_x I_{1,j+1/2} &= 0, \\ P_{j+1/2}(t_+^n) &= \frac{p_j^n + p_{j+1}^n}{2}, \end{aligned}$$

where the interface values $\kappa_{j+1/2}$ and $\rho_{k,j+1/2}$ are computed from $P_{j+1/2}(t)$ together with the arithmetic average (22) which defines $\alpha_{k,j+1/2}(t)$.

Remark 2. The numerical flux $P_{j+1/2}(t) = P(U_j(t), U_{j+1}(t))$ is consistent with the physical flux. This follows easily since assuming that $U_j(t) = U_{j+1}(t) = U(t)$ for $t \in [t^n, t^{n+1}]$ implies that we shall solve the ODE

$$\dot{P}_{j+1/2} = 0, \quad P_{j+1/2}(t_+^n) = \frac{p_j^n + p_{j+1}^n}{2} = p(t^n),$$

i.e., $P_{j+1/2}(t) = p(t^n) = p(t)$ for $t \in [t^n, t^{n+1}]$.

3.4. The numerical flux $F_{k,j+1/2}(t)$. We first recall that from the masses $m_{k,j}(t)$, which in turn depend on the numerical mass fluxes $F_{k,j+1/2}(t)$ via the mass conservation equations of (21), we obtain the pressure $p_j(t)$ as well as the volume fraction $\alpha_{k,j}(t)$ by using the relation (13). To give more room for incorporating several properties which are relevant for accurate and nonoscillatory approximations of the

pressure $p_j(t)$ and the volume fraction $\alpha_{k,j}(t)$, we suggest describing the numerical mass fluxes $F_k(t)$ as a combination of two different flux components, $F_k^D(t)$ and $F_k^A(t)$, respectively.

More precisely, we associate the mass flux component F_k^D with the pressure calculation $p = p(m_g, m_l)$ via the relation (13) while the F_k^A component is associated with the volume fraction calculation $\alpha_k = m_k/\rho_k(p(m_g, m_l))$. An important point here is to give an appropriate description of the balance between the two components F_k^D and F_k^A as well as to develop the F_k^D and F_k^A components themselves. The first point is discussed in the following while the latter is postponed until section 6 and section 7, respectively.

From (17) and (18) we see that the mass differentials dm_k can be split into a pressure component dp and a volume fraction component $d\alpha$. We now want to design numerical fluxes which are consistent with this splitting; i.e., we introduce a flux component F_p and F_α such that the mass fluxes F_l and F_g are given by

$$(24) \quad F_l = \alpha_l \frac{\partial \rho_l}{\partial p} F_p + \rho_l F_\alpha$$

and

$$(25) \quad F_g = \alpha_g \frac{\partial \rho_g}{\partial p} F_p - \rho_g F_\alpha.$$

The flux component F_p is associated with the pressure; hence it is natural to assign a diffusive mass flux F^D for stable approximation of pressure for the various waves. Inspired by the differential relation (14) we propose to give F_p the following form:

$$(26) \quad F_p = \kappa \rho_g F_l^D + \kappa \rho_l F_g^D.$$

Similarly, the flux component F_α is associated with the volume fraction. Hence we seek to assign a mass flux F^A such that an accurate resolution of the volume fraction variable can be obtained. Inspired by the differential relation (15), we propose to give F_α the following form:

$$(27) \quad F_\alpha = \kappa \frac{\partial \rho_g}{\partial p} \alpha_g F_l^A - \kappa \frac{\partial \rho_l}{\partial p} \alpha_l F_g^A.$$

Here we note that a subscript $j + 1/2$ is assumed on the fluxes and coefficients. Substituting (26) and (27) into (25) and (24) we obtain the final hybrid mass fluxes

$$(28) \quad F_l = \kappa \left(\rho_g \alpha_l \frac{\partial \rho_l}{\partial p} F_l^D + \rho_l \alpha_g \frac{\partial \rho_g}{\partial p} F_l^A + \rho_l \alpha_l \frac{\partial \rho_l}{\partial p} (F_g^D - F_g^A) \right)$$

and

$$(29) \quad F_g = \kappa \left(\rho_l \alpha_g \frac{\partial \rho_g}{\partial p} F_g^D + \rho_g \alpha_l \frac{\partial \rho_l}{\partial p} F_g^A + \rho_g \alpha_g \frac{\partial \rho_g}{\partial p} (F_l^D - F_l^A) \right).$$

The coefficient variables at $j + 1/2$ remain to be determined. We suggest finding these from the cell interface pressure $P_{j+1/2}(t)$ as well as the relation

$$\alpha_{j+1/2}(t) = \frac{1}{2}(\alpha_j(t) + \alpha_{j+1}(t)),$$

which is consistent with the treatment of the coefficients of the pressure evolution equation (23).

Remark 3. We remark that the consistency criterion

$$F_k(U, U) = f_k(U) = \rho_k \alpha_k v_k,$$

relating the physical flux f_k to the numerical flux F_k , is satisfied for the hybrid fluxes (28) and (29) provided the fluxes F_k^A and F_k^D are consistent. In particular, if $F_k^A = F_k^D$, the expressions (28) and (29) reduce to the trivial identity

$$F_k = F_k^A = F_k^D.$$

3.5. The numerical flux $G_{k,j+1/2}(t)$. In principle, one could envisage a hybridization similar to (28) and (29) for constructing the convective momentum flux $G_{k,j+1/2}(t)$. We will not pursue such ideas here. For purposes of simplicity, we instead seek a more straightforward construction of this convective flux, coupling it to the mass flux component F_k^A only. To emphasize this we use the superscript A, i.e.,

$$(30) \quad G_{k,j+1/2}(t) = G_{k,j+1/2}^A(t).$$

More precisely, we choose $G_{k,j+1/2}^A(t)$ to be consistent with the flux component $F_{k,j+1/2}^A(t)$ in the following sense: for a flow with velocities which are constant in space for the time interval $[t^n, t^{n+1}]$, that is,

$$(31) \quad v_{k,j}(t) = v_{k,j+1}(t) = v_k(t), \quad t \in [t^n, t^{n+1}],$$

we assume that $G_{k,j+1/2}^A(t)$ takes the form

$$(32) \quad G_{k,j+1/2}^A(t) = v_k(t) F_{k,j+1/2}^A(t),$$

where $F_{k,j+1/2}^A(t)$ is the numerical flux component introduced above and assumed to be consistent with the physical flux $f_k = \rho_k \alpha_k v_k$.

Remark 4. We remark that the consistency criterion

$$G_k(U, U) = g_k(U) = \rho_k \alpha_k v_k^2,$$

relating the numerical flux G_k to the physical flux g_k , is satisfied for G_k as given by (32) provided the numerical flux F_k^A is consistent with the physical flux f_k .

4. Further development of the mass flux $F_{k,j+1/2}(t)$. A main issue in the resolution of two-phase flow as described by the current model is to obtain an accurate resolution of mass fronts, i.e., slow-moving volume fraction waves. Hence, in the following we want to ensure that the mass fluxes $F_k^D(t)$ and $F_k^A(t)$ are constructed so that certain “good” properties in this respect are ensured for the resulting mass flux $F_k(t)$. Particularly, we shall identify a simple characterization of some properties which F_k^D and F_k^A should possess.

To identify this characterization, we consider the contact discontinuity given by

$$(33) \quad \begin{aligned} p_L &= p_R = p, \\ \alpha_L &\neq \alpha_R, \\ (v_g)_L &= (v_l)_L = (v_g)_R = (v_l)_R = v \end{aligned}$$

for the period $[t^n, t^{n+1}]$. All pressure terms vanish from the model (4)–(7), and it is seen that the solution to this initial value problem is simply that the discontinuity will propagate with the velocity v . The exact solution of the Riemann problem will then give the numerical mass flux

$$(34) \quad (\rho\alpha v)_{j+1/2} = \frac{1}{2}\rho(\alpha_L + \alpha_R)v - \frac{1}{2}\rho(\alpha_R - \alpha_L)|v|.$$

DEFINITION 1. A numerical flux F that satisfies (34) for the contact discontinuity (33) will in the following be termed a mass coherent flux.

4.1. A mass coherent flux F_k^A . The purpose of the flux component F_k^A is to ensure accuracy at volume fraction waves. A natural requirement for F_k^A is then that it should be mass coherent in the sense of Definition 1. We shall return to a more detailed specification in section 7 but at this stage it might be instructive to briefly mention two examples of numerical mass fluxes studied before for the two-fluid model [9], one which is mass coherent and one which is not mass coherent.

Two examples. In [9] we studied a FVS-type of scheme for the current two-phase model whose mass fluxes are given by

$$(35) \quad (\rho\alpha v)_{j+1/2} = (\rho\alpha)_L V^+(v_L, c_{j+1/2}) + (\rho\alpha)_R V^-(v_R, c_{j+1/2})$$

for each phase where $c_{j+1/2} = \max(c_L, c_R)$ and V^\pm are given by

$$V^\pm(v, c) = \begin{cases} \pm \frac{1}{4c}(v \pm c)^2 & \text{if } |v| \leq c, \\ \frac{1}{2}(v \pm |v|) & \text{otherwise.} \end{cases}$$

Here the parameter c controls the amount of numerical diffusion and is normally associated with the physical sound velocity for the system. This flux is not mass coherent according to Definition 1 and leads to poor resolution of mass fronts, as was clearly observed in [9].

In [9] we also studied a modification of the mass fluxes (35) obtained by replacing V^\pm by

$$\tilde{V}^\pm(v, c, \chi) = \begin{cases} \chi V^\pm(v, c) + (1 - \chi) \frac{v \pm |v|}{2}, & |v| < c, \\ \frac{1}{2}(v \pm |v|) & \text{otherwise,} \end{cases}$$

where χ_L and χ_R satisfy the relation

$$(36) \quad \chi_R \alpha_R - \chi_L \alpha_L = 0.$$

It is easy to verify that the resulting mass flux is mass coherent in the sense of Definition 1, and we observed in [9] that the level of accuracy was similar to that of a Roe scheme in the resolution of mass fronts.

Knowing that the total flux component F_k given by (28) and (29) also should be accurate at volume fraction waves, i.e., mass coherent, we may ask, What is a minimal condition satisfied by the F_k^D component which ensures that F_k still becomes mass coherent?

4.2. A pressure coherent flux F_k^D . We note that the pressure will remain constant and uniform as the discontinuity (33) is propagating. Consequently, a natural requirement on a good flux F_k^D for stable pressure resolution is that it preserves the constancy of pressure for the moving or stationary contact discontinuity given by (33).

We write (14) as

$$dp = \kappa d\mu,$$

where

$$(37) \quad d\mu = \rho_g dm_1 + \rho_l dm_g.$$

To maintain a constant pressure we must have $d\mu = 0$. Assuming constant pressure, (37) can be integrated to yield

$$\mu = \rho_g m_1 + \rho_l m_g = \rho_g \rho_l (\alpha_1 + \alpha_g) = \rho_g \rho_l.$$

To maintain constancy of μ , and hence p , we now insist that the flux F_k^D is a consistent numerical flux when applied to the mix mass μ . That is, we impose

$$(38) \quad \rho_g F_{1,j+1/2}^D + \rho_l F_{g,j+1/2}^D = \rho_g \rho_l v$$

for the contact discontinuity (33).

DEFINITION 2. *A pair of numerical fluxes (F_1, F_g) that satisfy (38) for the contact discontinuity (33) will in the following be termed pressure coherent fluxes.*

In particular, we note that the FVS mass fluxes (35) as well as the upwind fluxes (34) are pressure coherent. Thus, the class of mass coherent fluxes is contained in the class of pressure coherent fluxes. However, it should be noted that we can easily construct a pair of perfectly valid mass fluxes, in the sense that they are consistent with the physical flux, that are not pressure coherent. Consider, for example, the stationary contact discontinuity (33) with $v = 0$. Let F_g be given by the upwind flux (34) and let F_1 be given by the FVS flux (35). Then

$$\rho_g F_{1,j+1/2} + \rho_l F_{g,j+1/2} = \rho_g \rho_l \frac{c}{4} ((\alpha_1)_L - (\alpha_1)_R) \neq 0,$$

defying the requirement (38). Thus, this mass flux is neither pressure nor mass coherent in the sense of Definitions 1 and 2.

4.3. Construction of mass coherent fluxes $F_k(t)$. We now state the following important lemma.

LEMMA 1. *Let the mixture fluxes (28) and (29) be constructed from pressure coherent fluxes F_k^D in the sense of Definition 2 and mass coherent fluxes F_k^A in the sense of Definition 1. Then the hybrid fluxes (28) and (29) reduce to the upwind fluxes (34) on the contact discontinuity (33); i.e., they are mass coherent.*

Proof. We consider the hybrid liquid mass flux (28) and assume that $v \geq 0$. Remembering that a subscript $j + 1/2$ is assumed on the variables, we write the flux as

$$(39) \quad F_1 = \kappa \left(\alpha_1 \frac{\partial \rho_1}{\partial p} (\rho_g F_1^D + \rho_l F_g^D) + \rho_l \alpha_g \frac{\partial \rho_g}{\partial p} F_1^A - \rho_l \alpha_1 \frac{\partial \rho_l}{\partial p} F_g^A \right).$$

Using the required properties of F_k^A and F_k^D given by Definition 1 and Definition 2, respectively, we obtain

$$(40) \quad F_1 = \kappa \left(\alpha_1 \frac{\partial \rho_1}{\partial p} \rho_g \rho_l v + \rho_l^2 \alpha_g \frac{\partial \rho_g}{\partial p} (\alpha_1)_L v - \rho_g \rho_l \alpha_1 \frac{\partial \rho_l}{\partial p} (1 - (\alpha_1)_L) v \right) = \rho_l (\alpha_1)_L v,$$

where we have used that

$$(41) \quad \rho_{j+1/2} = \rho_L = \rho_R,$$

which follows from the assumption of constant, uniform pressure. Spatial and phasic symmetry directly give the corresponding results for F_g and $v \leq 0$, completing the proof. \square

Remark 5. The importance of Lemma 1 lies in the fact that it allows us to search for an appropriate flux component F_k^D outside the class of mass coherent fluxes, and still, as long as F_k^D is pressure coherent and F_k^A is mass coherent, we obtain mass coherent fluxes F_k . This is the crucial mechanism of the decomposition (28) and (29).

4.4. The class of MF methods. Motivated by the mixture mass fluxes (28) and (29) as well as the use of the pressure evolution equation (23), we propose the following definition.

DEFINITION 3. *We will use the term MF methods to denote numerical algorithms which are constructed within the above semidiscrete framework; that is, (i) the numerical mass flux $F_{k,j+1/2}(t)$ is given by the mixture fluxes (28) and (29), where F_k^D is pressure coherent in the sense of Definition 2 and F_k^A is mass coherent in the sense of Definition 1; (ii) the numerical pressure flux $P_{j+1/2}(t)$ is obtained as the solution of (23); and (iii) the convective flux $G_{k,j+1/2}^A(t)$ satisfies (32) for flow with uniform velocity (31).*

Next, we apply Lemma 1 to verify that the MF methods satisfy the following principle, due to Abgrall [1, 22, 23]: a flow, uniform in pressure and velocity, must remain uniform in the same variables during its time evolution.

LEMMA 2. *The MF methods given by Definition 3 obey Abgrall’s principle.*

Proof. We assume that we have the contact discontinuity given by (33) and that it remains unchanged during the time interval $[t^n, t^{n+1}]$. In view of Lemma 1 and the fact that the convective fluxes $G_{k,j+1/2}^A(t)$ of the momentum equations of the MF methods satisfy (32), we immediately conclude that the semidiscrete model (21) takes the form

$$(42) \quad \begin{aligned} \dot{m}_{k,j} + \delta_x(\rho_k \alpha_k v_k)_j &= 0, \\ v \dot{m}_{k,j} + v \delta_x(\rho_k \alpha_k v_k)_j + \alpha_{k,j} \delta_x P_j + (\Delta p)_j \delta_x \Lambda_{k,j} &= 0, \end{aligned}$$

where $(\rho_k \alpha_k v_k)_{j+1/2}$ is given by (34). In view of (11) we conclude that $(\Delta p)_j = 0$. Moreover, we see that (23) reduces to

$$\begin{aligned} \dot{P}_{j+1/2} &= -[\kappa_{j+1/2} \rho_{1,j+1/2}] \delta_x I_{g,j+1/2} + [\kappa_{j+1/2} \rho_{g,j+1/2}] \delta_x I_{1,j+1/2} \\ &= -\kappa_{j+1/2} [\rho_1 \rho_g v \delta_x \alpha_{g,j+1/2} + \rho_g \rho_1 v \delta_x \alpha_{1,j+1/2}] = 0 \end{aligned}$$

since $\alpha_g + \alpha_1 = 1$. In other words,

$$P_{j+1/2}(t) = P_{j+1/2}(t_+^n) = \frac{p_j^n + p_{j+1}^n}{2} = p, \quad t \in (t^n, t^{n+1}],$$

for all j . Consequently, $\delta_x P_j = 0$, and we can conclude that Abgrall’s principle holds for the MF methods. \square

Remark 6. We may consider the class of schemes introduced in this paper, which all employ mass fluxes of the form (28) and (29), as genuine *two-phase* flux splitting schemes. This flux splitting is based on a decomposition of the mass fluxes into several

phasic components, i.e., one specific mass flux involves components from both the liquid and the gas phase. In this sense the class of schemes we study is fundamentally different from the solution method used in, e.g., [4, 17, 18, 9], where the underlying philosophy is to solve the two-phase model basically as two single-phase problems.

In the next sections (sections 5, 6, and 7) we shall specify fully discrete schemes based on the semidiscrete scheme presented in sections 3 and 4. In particular, we will develop a flux component F_k^D which is pressure coherent but not mass coherent. This flux component is constructed so that it allows us to obtain a stable pressure $p = p(m_g, m_l)$ via (13), even for time steps which obey only the weak CFL condition (2). The fact that it is pressure coherent, i.e., satisfies (38) for a contact discontinuity (33), ensures that it does not introduce undesirable numerical dissipation at volume fraction waves. The construction of appropriate flux components F_k^A and G_k^A will be based on the advection upstream splitting method (AUSM) framework developed by Wada and Liou [28] for Euler equations and adapted to the two-phase flow model in [9]; see also [18] for similar types of schemes for the two-fluid model.

5. Fully discrete numerical schemes. We now consider a fully discrete scheme corresponding to the semidiscrete scheme given by (21), (22), (23), (28), (29), and (30).

General form.

- Gas mass,

$$(43) \quad \frac{m_{g,j}^{n+1} - m_{g,j}^n}{\Delta t} = -\delta_x F_{g,j}^{n+1/2};$$

- liquid mass,

$$(44) \quad \frac{m_{l,j}^{n+1} - m_{l,j}^n}{\Delta t} = -\delta_x F_{l,j}^{n+1/2};$$

- pressure at cell interface,

$$(45) \quad \begin{aligned} & \frac{P_{j+1/2}^{n+1} - \frac{1}{2}(p_j^n + p_{j+1}^n)}{\Delta t} \\ & = -(\kappa\rho_l)_{j+1/2}^n \frac{I_{g,j+1}^{n+1} - I_{g,j}^{n+1}}{\Delta x} - (\kappa\rho_g)_{j+1/2}^n \frac{I_{l,j+1}^{n+1} - I_{l,j}^{n+1}}{\Delta x}; \end{aligned}$$

- gas momentum,

$$(46) \quad \begin{aligned} & \frac{I_{g,j}^{n+1} - I_{g,j}^n}{\Delta t} \\ & = -\delta_x (G^A)_{g,j}^n - \alpha_{g,j}^n \frac{P_{j+1/2}^{n+1} - P_{j-1/2}^{n+1}}{\Delta x} - (\Delta p)_j^n \delta_x \Lambda_{g,j}^n + (Q_g)_j^n; \end{aligned}$$

- liquid momentum,

$$(47) \quad \begin{aligned} & \frac{I_{l,j}^{n+1} - I_{l,j}^n}{\Delta t} \\ & = -\delta_x (G^A)_{l,j}^n - \alpha_{l,j}^n \frac{P_{j+1/2}^{n+1} - P_{j-1/2}^{n+1}}{\Delta x} - (\Delta p)_j^n \delta_x \Lambda_{l,j}^n + (Q_l)_j^n. \end{aligned}$$

Here we have introduced the shorthand

$$m_k = \rho_k \alpha_k, \quad I_k = m_k v_k.$$

In accordance with (22) we use

$$(48) \quad \Lambda_{k,j+1/2}^n = \frac{\alpha_{k,j}^n + \alpha_{k,j+1}^n}{2},$$

and where $(\Delta p)_j^n = (\Delta p)(U_j^n, \delta)$ is evaluated from (11). For the discretization of the pressure evolution equation (23) as given by (45), we keep the coefficients $\kappa \rho_k$ fixed at time level t^n , whereas the mass fluxes I_k are given an implicit treatment as they are discretized at time level t^{n+1} . Particularly, this enforces a coupling between (45), (46), and (47). We end up with solving a linear system $Ax = b$, where A is a sparse banded matrix with two superdiagonals and two subdiagonals.

For the numerical mass fluxes $F_{k,j+1/2}^{n+1/2}$ the purpose of the $n + 1/2$ notation is to indicate that we shall discretize some terms at time level t^n and others at time t^{n+1} . More precisely, we propose to use the following time discretization for the mass fluxes (28) and (29) (for simplicity we have again dropped the subscript $j + 1/2$):

$$(49) \quad \begin{aligned} F_1^{n+1/2} &= [\kappa \rho_g \alpha_1(\rho_1)_p]^n (F_1^D)^{n+1/2} + [\kappa \rho_1 \alpha_g(\rho_g)_p]^n (F_1^A)^n \\ &\quad + [\kappa \rho_1 \alpha_1(\rho_1)_p]^n \left((F_g^D)^{n+1/2} - (F_g^A)^n \right) \end{aligned}$$

and

$$(50) \quad \begin{aligned} F_g^{n+1/2} &= [\kappa \rho_1 \alpha_g(\rho_g)_p]^n (F_g^D)^{n+1/2} + [\kappa \rho_g \alpha_1(\rho_1)_p]^n (F_g^A)^n \\ &\quad + [\kappa \rho_g \alpha_g(\rho_g)_p]^n \left((F_1^D)^{n+1/2} - (F_1^A)^n \right). \end{aligned}$$

In other words, the flux component F_k^A is kept at the time level t^n , whereas the flux component F_k^D involves terms at time level t^{n+1} . Particularly, we want to make use of the updated momentums I_k^{n+1} obtained from solving (45)–(47) in the expressions for F_k^D . We describe the details in the next section.

It turns out that this implicit treatment is crucial to maintain the stability of the scheme for large time steps. This aspect is explored in more detail in section 8.1. Note that we shall not need to solve any linear system here, as will become clear from section 6. In view of (49) and (50), we see that what remains is to specify the numerical flux components $(F_k^A)_{j+1/2}^n$ and $(G_k^A)_{j+1/2}^n$, as well as $(F_k^D)_{j+1/2}^{n+1/2}$. We start with the latter.

Remark 7. The discretization of the pressure equation at the cell interface can be viewed as a staggered Lax–Friedrichs scheme. We assume that the pressure p_j is found from the masses m_j by (13). The interdependence between $P_{j+1/2}$ and the couple (p_j, p_{j+1}) through the proposed discretization (45) ensures that the numerical flux $P_{j+1/2}$ is consistent with the physical flux, as pointed out in Remark 2.

6. Specification of the pressure coherent convective flux $(F_k^D)^{n+1/2}$. Due to the fact that the mass flux component F_k^D is associated with the pressure calculation as described in section 3.4, it is natural to choose a discretization of this flux which is consistent with the discretization of the pressure evolution equation. On

the semidiscrete level, in view of (23), we therefore propose to consider the following discretization of the mass conservation equations:

$$(51) \quad \begin{aligned} \dot{m}_{k,j+1/2} + \delta_x I_{k,j+1/2} &= 0, \quad t \in (t^n, t^{n+1}], \\ m_{k,j+1/2}(t_+^n) &= \frac{m_{k,j}^n + m_{k,j+1}^n}{2}. \end{aligned}$$

We now suggest averaging as follows:

$$m_{k,j}(t) = \frac{1}{2} (m_{k,j-1/2}(t) + m_{k,j+1/2}(t)),$$

which implies that

$$(52) \quad \dot{m}_{k,j}(t) = \frac{1}{2} (\dot{m}_{k,j-1/2}(t) + \dot{m}_{k,j+1/2}(t)).$$

By substituting (51) into (52) we obtain the following ODE equation for $m_{k,j}(t)$:

$$(53) \quad \begin{aligned} \dot{m}_{k,j} + \frac{1}{2\Delta x} (I_{k,j+1} - I_{k,j-1}) &= 0, \quad t \in (t^n, t^{n+1}], \\ m_{k,j}(t_+^n) &= \frac{1}{4} (m_{k,j-1}^n + 2m_{k,j}^n + m_{k,j+1}^n). \end{aligned}$$

To achieve conservative mass treatment while maintaining CFL stability, it is clear that we somehow should take advantage of the already implicitly calculated mass fluxes $I_{k,j}^{n+1}$ obtained from solving (45)–(47). A fully discrete version of (53) which employs these updated mass fluxes $I_{k,j}^{n+1}$ is then given by

$$(54) \quad \frac{m_{k,j}^{n+1} - \frac{1}{4} (2m_{k,j}^n + m_{k,j-1}^n + m_{k,j+1}^n)}{\Delta t} + \frac{1}{2\Delta x} (I_{k,j+1}^{n+1} - I_{k,j-1}^{n+1}) = 0,$$

which can be written in flux-conservative form (43) and (44) with the numerical fluxes

$$(55) \quad (F_k^D)_{j+1/2}^{n+1/2} = \frac{1}{2} (I_{k,j}^{n+1} + I_{k,j+1}^{n+1}) + \frac{1}{4} \frac{\Delta x}{\Delta t} (m_{k,j}^n - m_{k,j+1}^n).$$

Now we may solve for the masses $m_{k,j}^{n+1}$ using the fluxes (55), taking advantage of the fact that they emerge through an implicit coupling to the pressure. We found that by doing this we were able to violate the CFL criterion for sonic waves. This is explored in more detail in section 8.1.

Next, we check that the proposed flux F_k^D possesses the pressure coherent property of Definition 2.

PROPOSITION 1. *The flux component F_k^D given by (55) is pressure coherent in the sense of Definition 2.*

Proof. We just need to check that F_k^D satisfies the relation (38). Using the constants of (33), a direct calculation gives

$$\begin{aligned} \rho_g (F_1^D)_{j+1/2}^{n+1/2} + \rho_l (F_g^D)_{j+1/2}^{n+1/2} &= \rho_g \rho_l \left[\frac{v}{2} (\alpha_{1,j}^{n+1} + \alpha_{1,j+1}^{n+1}) + \frac{\Delta x}{4\Delta t} (\alpha_{1,j}^n - \alpha_{1,j+1}^n) \right] \\ &\quad + \rho_g \rho_l \left[\frac{v}{2} (\alpha_{g,j}^{n+1} + \alpha_{g,j+1}^{n+1}) + \frac{\Delta x}{4\Delta t} (\alpha_{g,j}^n - \alpha_{g,j+1}^n) \right] \\ &= \rho_g \rho_l \left[\frac{v}{2} (1 + 1) + \frac{\Delta x}{4\Delta t} (1 - 1) \right] = \rho_g \rho_l v. \quad \square \end{aligned}$$

Note, however, by direct calculation, that this F_k^D mass flux component is not mass coherent in the sense of Definition 1.

Remark 8. Our experience is that it is essential to use a discretization of the mass equations, represented by the F_k^D flux component (55), which is consistent with the one used for the pressure evolution equation to obtain nonoscillatory (stable) approximations for the pressure when large time steps governed by (2) are employed. However, this leads to mass fluxes F_k^D which are not mass coherent according to Definition 1.

Consequently, by using F_k^D only as mass fluxes, i.e., $F_k = F_k^D$, we must expect that a strong smearing of volume fraction waves is introduced. However, Lemma 1 states that by the introduction of the mixture mass fluxes (28) and (29) we only need F_k^D to satisfy the weaker pressure coherent condition given by Definition 2, and still we retain mass fluxes F_k which are mass coherent as long as we use a mass coherent F_k^A component.

7. Specification of the mass coherent convective fluxes (F_k^A)ⁿ and corresponding convective momentum fluxes (G_k^A)ⁿ. In this section we look for appropriate choices for the numerical flux components F_k^A and G_k^A by considering so-called hybrid FDS/FVS types of schemes. Such schemes have been explored for the present two-fluid model [9]. Here we briefly restate the numerical convective fluxes $(\rho\alpha v)_{j+1/2}$ and $(\rho\alpha v^2)_{j+1/2}$ corresponding to the flux splitting schemes we investigated in [9].

7.1. FVS/van Leer. We consider the velocity splitting formulas used in previous works [13, 28, 7, 8, 9]:

$$(56) \quad V^\pm(v, c) = \begin{cases} \pm \frac{1}{4c}(v \pm c)^2 & \text{if } |v| \leq c, \\ \frac{1}{2}(v \pm |v|) & \text{otherwise.} \end{cases}$$

Here the parameter c controls the amount of numerical diffusion and is normally associated with the physical sound velocity for the system. Following [9] we here assume that the sound velocity is given by (12). Following the standard set by earlier works [28, 7, 9] we choose a common sound velocity

$$c_{j+1/2} = \max(c_L, c_R)$$

at the cell interface.

1. *Mass flux.* We let the numerical mass flux $(\rho\alpha v)_{j+1/2}$ for FVS and van Leer be given as

$$(57) \quad (\rho\alpha v)_{j+1/2} = (\rho\alpha)_L V^+(v_L, c_{j+1/2}) + (\rho\alpha)_R V^-(v_R, c_{j+1/2})$$

for each phase.

2. *Momentum flux.* We let the numerical convective momentum flux $(\rho\alpha v^2)_{j+1/2}$ be given as

- FVS,

$$(58) \quad (\rho\alpha v^2)_{j+1/2} = V^+(v_L, c_{j+1/2})(\rho\alpha v)_L + V^-(v_R, c_{j+1/2})(\rho\alpha v)_R,$$

- van Leer,

$$(59) \quad (\rho\alpha v^2)_{j+1/2} = \frac{1}{2}(\rho\alpha v)_{j+1/2}(v_L + v_R) - \frac{1}{2}|(\rho\alpha v)_{j+1/2}|(v_R - v_L).$$

7.2. AUSMV/AUSMD. Following [9], we consider the convective fluxes associated with the AUSMV and AUSMD scheme obtained by replacing the splitting formulas V^\pm used in (57)–(59) with the less diffusive pair

$$(60) \quad \tilde{V}^\pm(v, c, \chi) = \begin{cases} \chi V^\pm(v, c) + (1 - \chi) \frac{v \pm |v|}{2}, & |v| < c, \\ \frac{1}{2}(v \pm |v|) & \text{otherwise,} \end{cases}$$

where

$$(61) \quad \chi_L = \frac{2(\rho/\alpha)_L}{(\rho/\alpha)_L + (\rho/\alpha)_R}$$

and

$$(62) \quad \chi_R = \frac{2(\rho/\alpha)_R}{(\rho/\alpha)_L + (\rho/\alpha)_R}$$

for each phase.

DEFINITION 4. *Using the terminology of Wada and Liou [28], we will henceforth refer to the FVS scheme modified with the splittings (60) and the choice of χ described by (61) and (62) as the AUSMV scheme. That is, the convective fluxes of AUSMV are described by*

- mass flux,

$$(63) \quad (\rho\alpha v)_{j+1/2}^{\text{AUSMV}} = (\rho\alpha)_L \tilde{V}^+(v_L, c_{j+1/2}, \chi_L) + (\rho\alpha)_R \tilde{V}^-(v_R, c_{j+1/2}, \chi_R),$$

- momentum flux,

$$(64) \quad (\rho\alpha v^2)_{j+1/2}^{\text{AUSMV}} = \tilde{V}^+(v_L, c_{j+1/2}, \chi_L)(\rho\alpha v)_L + \tilde{V}^-(v_R, c_{j+1/2}, \chi_R)(\rho\alpha v)_R.$$

DEFINITION 5. *Similarly, we will henceforth refer to the van Leer scheme modified with the splittings (60) and the choice of χ described by (61) and (62) as the AUSMD scheme. That is, the convective fluxes of AUSMD are described by*

- mass flux,

$$(65) \quad (\rho\alpha v)_{j+1/2}^{\text{AUSMD}} = (\rho\alpha)_L \tilde{V}^+(v_L, c_{j+1/2}, \chi_L) + (\rho\alpha)_R \tilde{V}^-(v_R, c_{j+1/2}, \chi_R),$$

- momentum flux,

$$(66) \quad (\rho\alpha v^2)_{j+1/2}^{\text{AUSMD}} = \frac{1}{2}(\rho\alpha v)_{j+1/2}(v_L + v_R) - \frac{1}{2}|(\rho\alpha v)_{j+1/2}|(v_R - v_L).$$

We note that χ_L and χ_R given by (61) and (62) satisfy the relation (36). Consequently, as remarked in section 4.1, it is easy to check by direct calculation that the AUSMV and AUSMD convective fluxes hold the following property; see also [9].

PROPOSITION 2. *The convective fluxes $(\rho\alpha v)_{j+1/2}^{\text{AUSMV}}$ and $(\rho\alpha v)_{j+1/2}^{\text{AUSMD}}$ are mass coherent in the sense of Definition 1.*

7.3. WIMF-AUSMD and WIMF-AUSMV. We are now in a position where we can give a precise definition of fully discrete MF schemes. We shall consider the following two different choices for $(F_k^A)^n$ and $(G_k^A)^n$ leading to two different MF schemes.

DEFINITION 6. We will use the term *WIMF-AUSMV* to denote the numerical scheme given by (43)–(50), where $(F_k^D)_{j+1/2}^{n+1/2}$ is given by the pressure coherent component (55) whereas $(F_k^A)_{j+1/2}^n$ and $(G_k^A)_{j+1/2}^n$ are given by

$$(F_k^A)_{j+1/2}^n = (\rho\alpha v)_{k,j+1/2}^{\text{AUSMV},n}, \quad (G_k^A)_{j+1/2}^n = (\rho\alpha v^2)_{k,j+1/2}^{\text{AUSMV},n}.$$

DEFINITION 7. We will use the term *WIMF-AUSMD* to denote the numerical scheme given by (43)–(50), where $(F_k^D)_{j+1/2}^{n+1/2}$ is given by the pressure coherent component (55) whereas $(F_k^A)_{j+1/2}^n$ and $(G_k^A)_{j+1/2}^n$ are given by

$$(F_k^A)_{j+1/2}^n = (\rho\alpha v)_{k,j+1/2}^{\text{AUSMD},n}, \quad (G_k^A)_{j+1/2}^n = (\rho\alpha v^2)_{k,j+1/2}^{\text{AUSMD},n}.$$

The following result holds for WIMF-AUSMV and WIMF-AUSMD.

PROPOSITION 3. *WIMF-AUSMV and WIMF-AUSMD satisfy the following properties: (i) The mass fluxes of WIMF-AUSMV and WIMF-AUSMD are mass coherent in the sense of Definition 1, and (ii) both schemes obey Abgrall's principle.*

Proof. In view of Lemma 1, result (i) follows directly from Proposition 1 and Proposition 2.

Result (ii) follows by observing that the flux component G_k^A of both schemes (see Definitions 6 and 7) satisfy the relation (32) for flow with uniform velocity (31) and then by applying Lemma 2. \square

Remark 9. We observed in [9] that the convective fluxes of AUSMV were considerably more diffusive on volume fraction waves than those of AUSMD. Thus, for numerical simulations we prefer to use the WIMF-AUSMD scheme which applies AUSMD mass and momentum fluxes for F_k^A and G_k^A , respectively. However, we will take advantage of the robustness of the convective fluxes of AUSMV and apply these in combination with the convective fluxes of AUSMD in an appropriate manner when we consider flows which locally involve transition to single-phase flow. We refer to section 8.3 for details.

8. Numerical simulations. In the following, some selected numerical examples will be presented. We will consider the performance of the WIMF-AUSMD scheme given by Definition 7. To ensure that this scheme can handle flow cases which involve transition to single-phase flow, we introduce a slight modification whose basic purpose is to introduce more numerical dissipation near the single-phase zone. This is explained in detail in section 8.3.

As our main concern will be to demonstrate the inherent accuracy and stability properties of the WIMF-AUSMD scheme, we limit ourselves to first-order accuracy in space and time. The boundary conditions are implemented using a simple ghost cell approach, where the variables are either imposed or determined by simple (zeroth-order) extrapolation from the computational domain.

In the first example we explore more carefully central mechanisms of the WIMF-AUSMD scheme.

8.1. A large relative velocity shock. We consider a Riemann initial value problem investigated by Cortes, Debussche, and Toumi [5] for a similar two-fluid model. Our primary motivation for studying this problem is to investigate the performance of WIMF-AUSMD on sonic waves. The initial states are given by

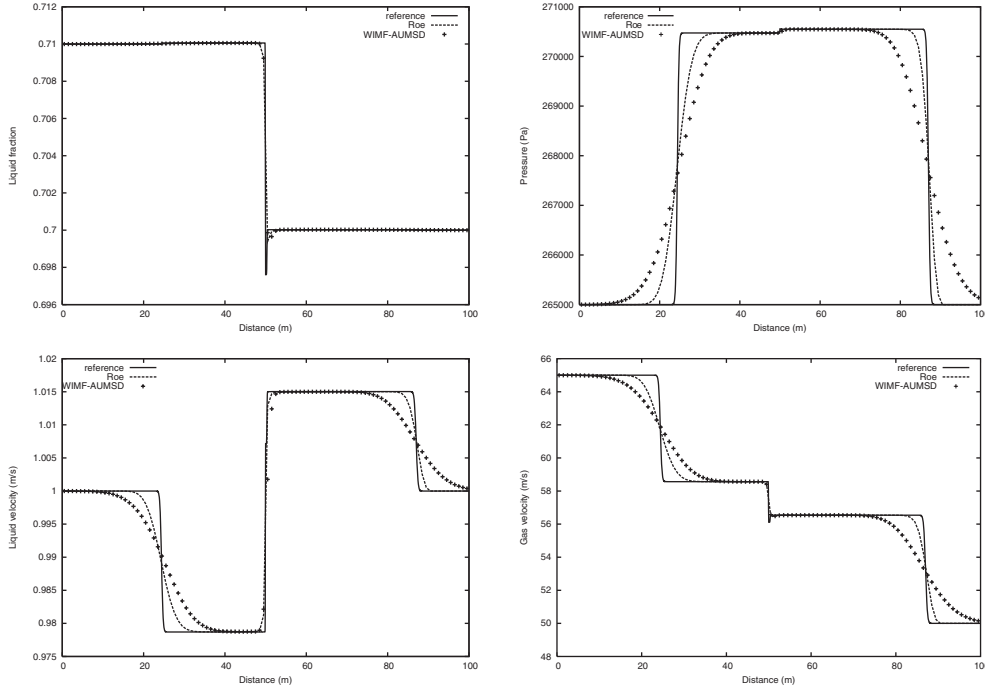


FIG. 1. LRV shock tube problem. WIMF-AUSMD versus Roe scheme for a grid of 100 cells. Top left: liquid fraction. Top right: pressure. Bottom left: liquid velocity: Bottom right: gas velocity.

$$(67) \quad \mathbf{W}_L = \begin{bmatrix} p \\ \alpha_1 \\ v_g \\ v_l \end{bmatrix} = \begin{bmatrix} 265000 \text{ Pa} \\ 0.71 \\ 65 \text{ m/s} \\ 1 \text{ m/s} \end{bmatrix}$$

and

$$(68) \quad \mathbf{W}_R = \begin{bmatrix} p \\ \alpha_1 \\ v_g \\ v_l \end{bmatrix} = \begin{bmatrix} 265000 \text{ Pa} \\ 0.7 \\ 50 \text{ m/s} \\ 1 \text{ m/s} \end{bmatrix}.$$

8.1.1. Comparison with explicit scheme. We aim here to compare the WIMF-AUSMD with an explicit Roe scheme at the same spatial and temporal grid. We refer to [9] for a description of the implementation of the Roe scheme. We assume a grid of 100 cells and use the time step

$$(69) \quad \frac{\Delta x}{\Delta t} = 400 \text{ m/s.}$$

The results, plotted at time $t = 0.1$ s, are given in Figure 1. The reference solution was computed using the Roe scheme on a grid of 10,000 cells.

We note that the implicit pressure-momentum coupling used in WIMF-AUMSD causes a stronger numerical dissipation associated with the sonic waves as compared to the explicit Roe scheme, whereas the approximation of the volume fraction waves

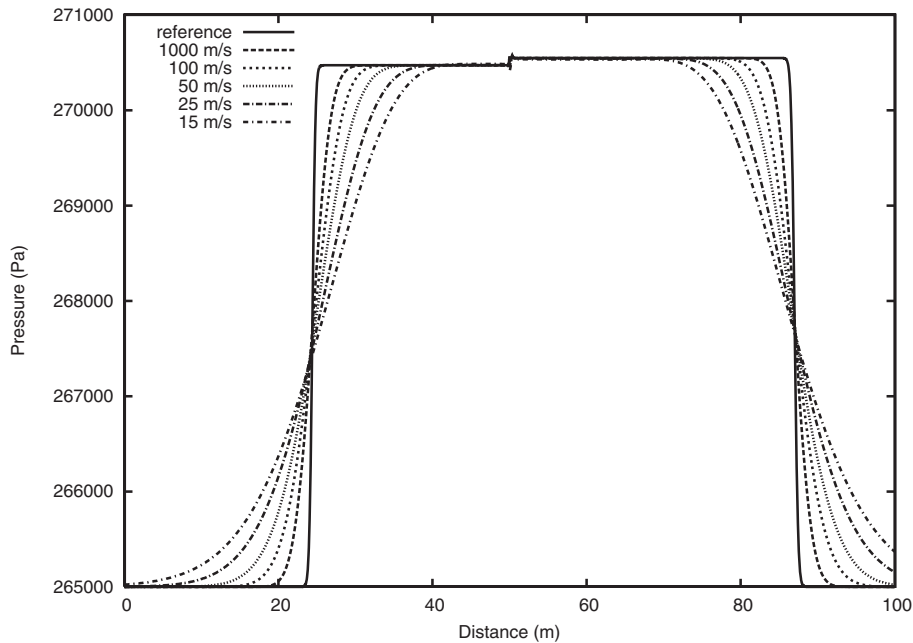


FIG. 2. LRV shock tube problem. Pressure is shown for a grid of 1000 cells. Different time steps are considered by considering different values for $\Delta x/\Delta t$ for the WIMF-AUSMD scheme.

located at about 50 m seems to be very similar. The approximation properties regarding the slow volume fraction waves for WIMF-AUSMD are explored in more detail in section 8.2 (water faucet problem).

8.1.2. Test of time step sensitivity for calculation of pressure using the WIMF-AUSMD scheme. We now investigate what happens when the time step is increased beyond the sonic CFL criterion. The two-fluid model possesses an approximate mixture velocity of sound given by

$$(70) \quad c = \sqrt{\frac{\rho_1 \alpha_g + \rho_g \alpha_1}{\frac{\partial \rho_g}{\partial p} \rho_1 \alpha_g + \frac{\partial \rho_1}{\partial p} \rho_g \alpha_1}}$$

(see [26, 9] for details). Hence the mixture sound velocity is approximately given by the sound velocity of the gas phase, giving

$$(71) \quad c \approx 317 \text{ m/s.}$$

Hence for time steps satisfying

$$(72) \quad \frac{\Delta x}{\Delta t} < c,$$

the sonic CFL criterion is broken. For a grid of 1000 cells, the results of the pressure calculation for several different values of $\Delta x/\Delta t$ are given in Figure 2. We observe that increasing the time step beyond the sonic CFL criterion (1) does not induce instabilities. However, a significant increase of the numerical dissipation of the sonic waves follows the increased time step.

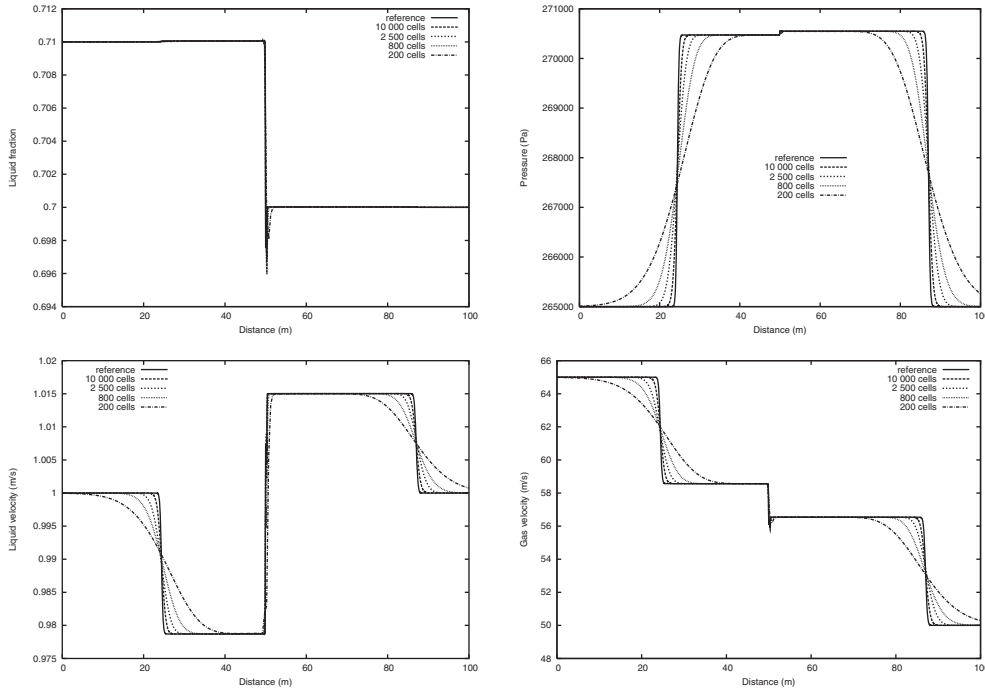


FIG. 3. LRV shock tube problem. Grid refinement for the WIMF-AUSMD scheme. Top left: liquid fraction. Top right: pressure. Bottom left: liquid velocity. Bottom right: gas velocity.

8.1.3. Test of stability and convergence for the WIMF-AUSMD scheme under violation of sonic CFL condition. Using the time step $\Delta x/\Delta t = 100$ m/s, the effect of grid refinement for the WIMF-AUSMD scheme is demonstrated in Figure 3. We observe that the Roe reference solution is approached in a monotone way and by that verifies that the stability of the WIMF-AUSMD scheme is not governed by the maximal speed of the sonic waves.

8.1.4. Test of using purely explicit mass fluxes F_k . We now wish to illustrate the need for using the implicitly calculated mass fluxes I_k^{n+1} as given by (55) when we approximate the mass equations. We consider a slight modification of the flux component F_k^D given by (55), where we instead use the momentum from the previous time step as follows:

$$(F_k^D)_{j+1/2}^n = \frac{1}{2}(I_{k,j}^n + I_{k,j+1}^n) + \frac{1}{4} \frac{\Delta x}{\Delta t} (m_{k,j}^n - m_{k,j+1}^n).$$

Results are given in Figure 4 for the time steps $\Delta x/\Delta t = 1000$ m/s and $\Delta x/\Delta t = 100$ m/s using a grid of 1000 cells. We observe that this works well for $\Delta x/\Delta t = 1000$ m/s when the sonic CFL condition is satisfied. However, increasing the time step by an order of magnitude leads to CFL-like instabilities, although the pressure-momentum coupling still is implicit. It seems to be a crucial step to use information from time level t^{n+1} to achieve stable mass calculations.

Remark 10. In particular, these results illustrate that the combination of using the pressure evolution equation (45) and the mixture mass fluxes (49) and (50), where $(F_k^D)^{n+1/2}$ is given by (55), makes the pressure calculation independent of any sonic CFL condition.

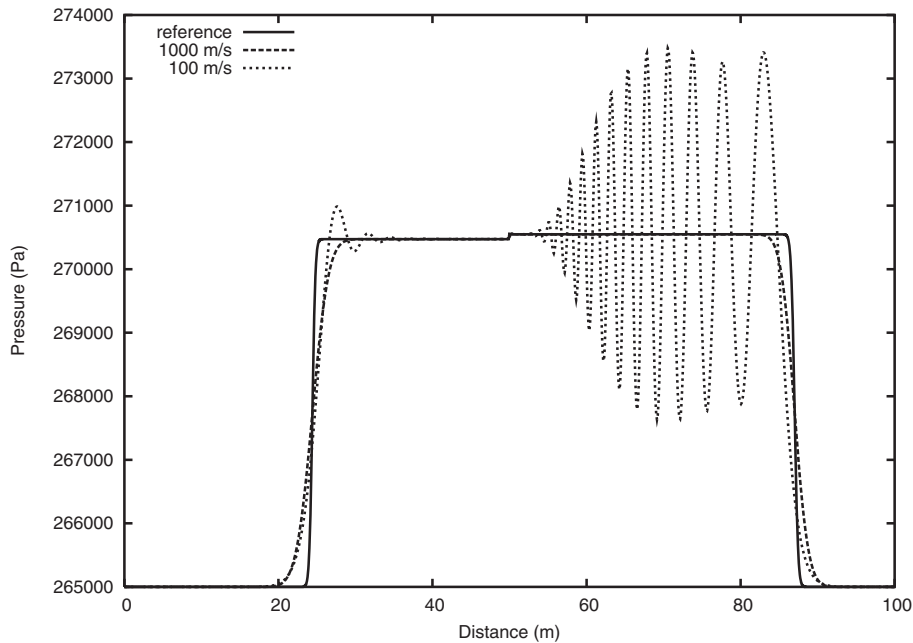


FIG. 4. LRV shock tube problem, 1000 cells. Modified WIMF-AUSMD. Purely explicit mass fluxes are used.

The strength of the mixture fluxes (49) and (50) lies in their ability to properly combine the stability of an implicit scheme with the accuracy of an explicit scheme, at least for the resolution of volume fraction waves. This is the central issue in the next example.

8.2. Water faucet problem. We now wish to focus more on the resolution of volume fraction waves. For this purpose, we study the faucet flow problem of Ransom [20], which has become a standard benchmark [27, 26, 4, 17, 18].

We consider a vertical pipe of length 12 m with the initial uniform state

$$(73) \quad \mathbf{W} = \begin{bmatrix} p \\ \alpha_1 \\ v_g \\ v_l \end{bmatrix} = \begin{bmatrix} 10^5 \text{ Pa} \\ 0.8 \\ 0 \\ 10 \text{ m/s} \end{bmatrix}.$$

Gravity is the only source term taken into account, i.e., in the framework of (6) and (7) we have

$$(74) \quad Q_k = g\rho_k\alpha_k,$$

with g being the acceleration of gravity. At the inlet we have the constant conditions $\alpha_1 = 0.8$, $v_l = 10$ m/s, and $v_g = 0$. At the outlet the pipe is open to the ambient pressure $p = 10^5$ Pa.

We restate the approximate analytical solution presented in [18, 27],

$$(75) \quad v_l(x, t) = \begin{cases} \sqrt{v_0^2 + 2gx} & \text{for } x < v_0t + \frac{1}{2}gt^2, \\ v_0 + gt & \text{otherwise,} \end{cases}$$

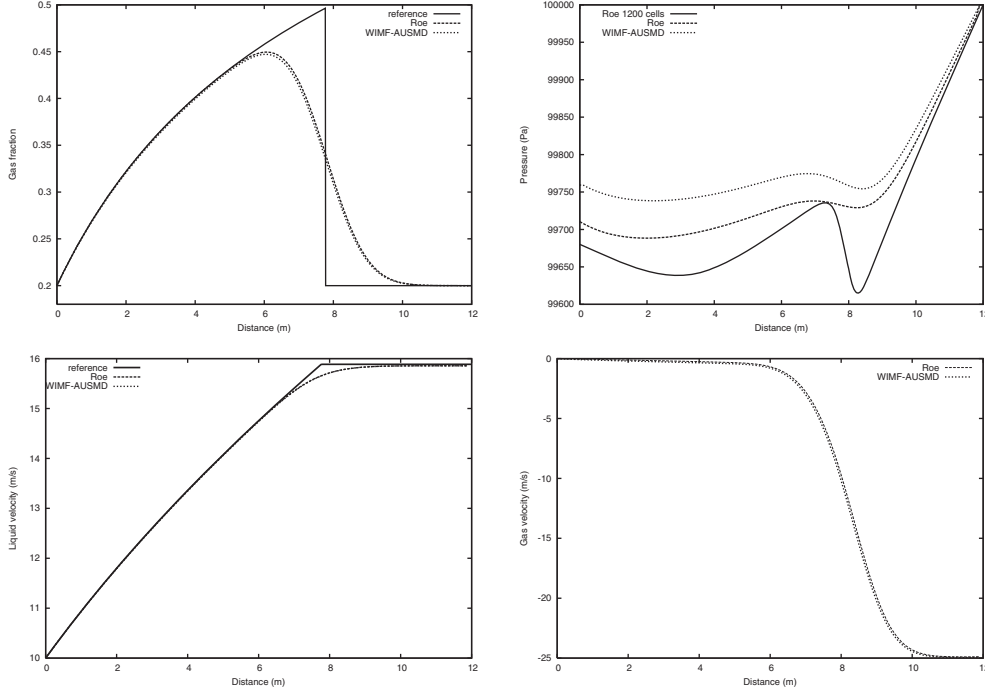


FIG. 5. Water faucet problem, 120 cells, $T = 0.6$ s. Roe versus WIMF-AUSMD, $\Delta x/\Delta t = 10^3$ m/s. Top left: gas fraction. Top right: pressure. Bottom left: liquid velocity. Bottom right: gas velocity.

$$(76) \quad \alpha_1(x, t) = \begin{cases} \alpha_0(1 + 2gxv_0^{-2})^{-1/2} & \text{for } x < v_0t + \frac{1}{2}gt^2, \\ \alpha_0 & \text{otherwise,} \end{cases}$$

where the parameters $\alpha_0 = 0.8$ and $v_0 = 10$ m/s are the initial states.

8.2.1. Comparison with explicit Roe scheme. We now compare the WIMF-AUSMD scheme with the explicit Roe scheme under equal conditions. That is, we assume a grid of 120 cells and use the time step

$$(77) \quad \frac{\Delta x}{\Delta t} = 10^3 \text{ m/s.}$$

Results are given in Figure 5 after $t = 0.6$ s. We note that there is little visible difference between WIMF-AUSMD and the Roe scheme on the volume fraction wave. However, the WIMF-AUSMD is somewhat more diffusive on pressure. This is consistent with our observations in section 8.1.1.

8.2.2. Effect of increasing the time step for WIMF-AUSMD. An eigenvalue analysis (see [26, 9]) reveals that the velocities of the volume fraction waves are approximately given by

$$(78) \quad \lambda_v^\pm = \frac{\rho_g \alpha_1 v_g + \rho_l \alpha_g v_l}{\rho_g \alpha_1 + \rho_l \alpha_g} \pm \sqrt{\frac{\Delta p (\rho_g \alpha_1 + \rho_l \alpha_g) - \rho_l \rho_g \alpha_1 \alpha_g (v_g - v_l)^2}{(\rho_g \alpha_1 + \rho_l \alpha_g)^2}}.$$

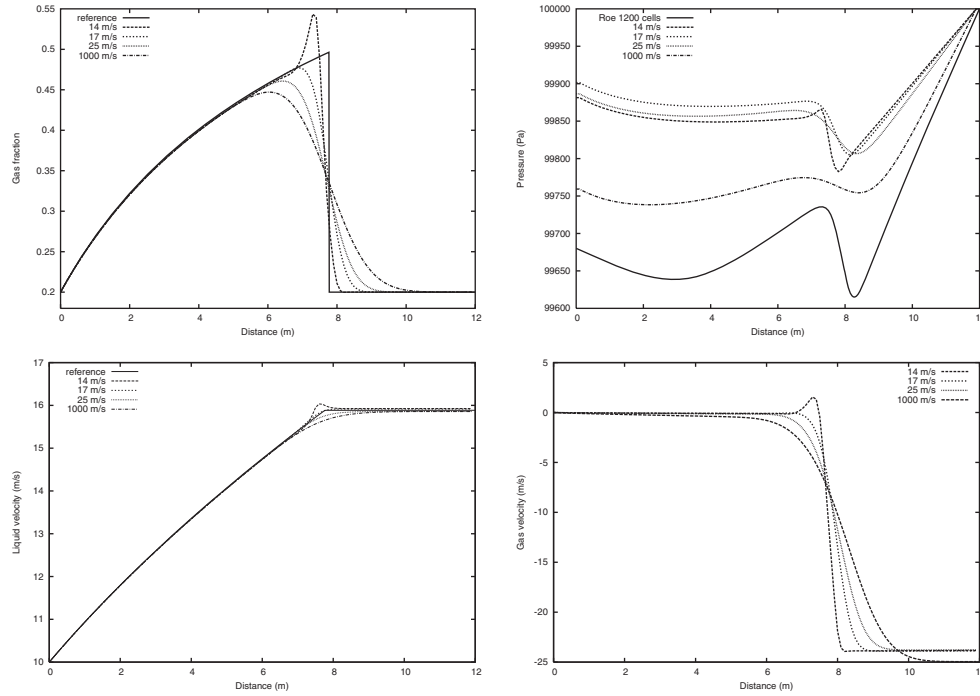


FIG. 6. Water faucet problem, 120 cells, $T = 0.6$ s. Different time steps for the WIMF-AUSMD scheme. Top left: gas fraction. Top right: pressure. Bottom left: liquid velocity. Bottom right: gas velocity.

For a weakly implicit scheme as defined by (2) we must then have

$$(79) \quad \frac{\Delta x}{\Delta t} \geq \max_{j,n}(\lambda_v^\pm).$$

Having $\rho_l \gg \rho_g$ we obtain from (78)

$$(80) \quad \lambda_v^\pm \approx v_l,$$

and hence we expect a weakly implicit scheme to encounter CFL-related stability problems near time steps corresponding to the liquid velocity.

We now study the effect of increasing the time step for the WIMF-AUSMD scheme. We consider the following time steps:

- $\Delta x/\Delta t = 1000$ m/s,
- $\Delta x/\Delta t = 25$ m/s,
- $\Delta x/\Delta t = 17$ m/s,
- $\Delta x/\Delta t = 14$ m/s.

Results for these time steps are given in Figure 6. We observe that increasing the time step toward the time step corresponding to the liquid velocity significantly improves the accuracy of WIMF-AUSMD on the volume fraction wave, as seen on the plots of velocities and volume fraction. The rate of improvement in accuracy is largest near the optimal time step $\Delta x/\Delta t = v_l$. Increasing the time step further violates the weak CFL criterion (79) and instabilities occur. The increased accuracy in volume fraction is accompanied by increased numerical dissipation in the pressure variable, consistent with our observations in section 8.1.2.

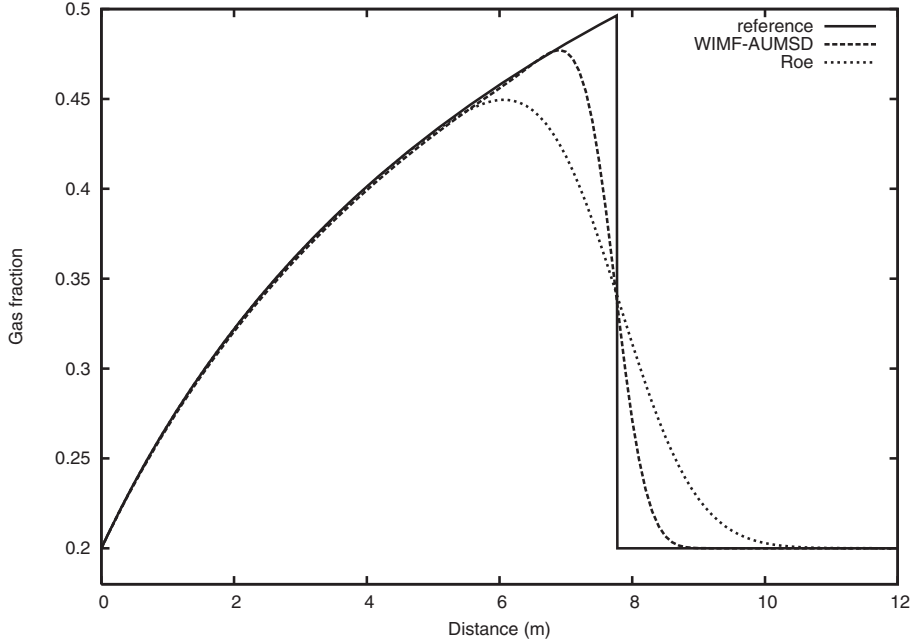


FIG. 7. Water faucet problem, $T = 0.6$ s, 120 grid cells. WIMF-AUSMD with optimal time step versus explicit Roe scheme.

8.2.3. Optimal WIMF-AUSMD versus Roe scheme. To emphasize the increased accuracy in volume fraction that is allowed by increasing the time step beyond the sonic CFL criterion, the explicit Roe scheme at $\Delta x/\Delta t = 1000$ m/s is plotted together with the optimal WIMF-AUSMD scheme ($\Delta x/\Delta t = 17$ m/s) in Figure 7. The improvement of the WIMF-AUSMD scheme is rather striking and is equivalent to an increase in the number of grid cells by an order of magnitude for the Roe scheme.

8.2.4. Test of convergence for WIMF-AUSMD. In Figure 8 we investigate how the scheme converges to the expected analytical solution as the grid is refined. The optimal time step $\Delta x/\Delta t = 17$ m/s is used. As we can see, the expected analytical solution is approached in a nonoscillatory way.

8.3. Separation problem. We consider a gravity-induced phase separation problem introduced by Coquel et al. [4] and also investigated by Paillère, Corre, and Cascales [18]. This problem tests the ability of numerical schemes to handle the transition to one-phase flow under stiff conditions.

We assume a vertical pipe of length 7.5 m, where gravitational acceleration and possibly interfacial friction are the source terms taken into account. Initially the pipe is filled with stagnant liquid and gas with a uniform pressure $p_0 = 10^5$ Pa and a uniform liquid fraction $\alpha_1 = 0.5$.

Assuming that the liquid column falls freely under the influence of gravity, the following approximate analytical solution can be derived for the transient period:

$$(81) \quad v_1(x, t) = \begin{cases} \sqrt{2gx} & \text{for } x < \frac{1}{2}gt^2, \\ gt & \text{for } \frac{1}{2}gt^2 \leq x < L - \frac{1}{2}gt^2, \\ 0 & \text{for } L - \frac{1}{2}gt^2 < x, \end{cases}$$

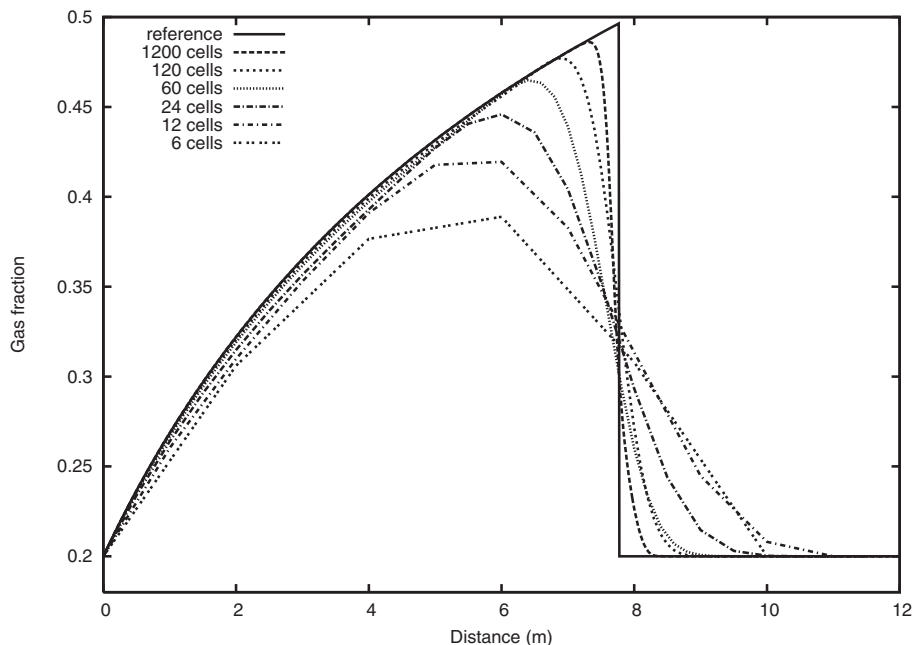


FIG. 8. Water faucet problem, $T = 0.6$ s. Grid refinement for the WIMF-AUSMD scheme.

$$(82) \quad \alpha_1(x, t) = \begin{cases} 0 & \text{for } x < \frac{1}{2}gt^2, \\ 0.5 & \text{for } \frac{1}{2}gt^2 \leq x < L - \frac{1}{2}gt^2, \\ 1 & \text{for } L - \frac{1}{2}gt^2 < x, \end{cases}$$

where $L = 7.5$ m is the length of the tube. This approximate solution consists of a contact discontinuity at the top of the tube and a shock-like discontinuity at the lower part of the tube. After the time

$$(83) \quad T = \sqrt{\frac{L}{g}} = 0.87 \text{ s}$$

these discontinuities will merge and the phases will become fully separated. The volume fraction reaches a stationary state, whereas the other variables slowly converge toward a stationary solution. Assuming hydrostatic conditions the pressure will approximately be given by

$$(84) \quad p(x, t) = \begin{cases} p_0 & \text{for } x < L/2, \\ p_0 + \rho_1 g(x - L/2) & \text{for } x \geq L/2. \end{cases}$$

8.3.1. Transition to one-phase flow. We observed that the basic WIMF-AUSMD scheme would produce instabilities in the transition to one-phase flow. Indeed, this is a common problem for two-phase flow models, observed by, among others, Coquel et al. [4] for their kinetic scheme, Paillère, Corre, and Cascales [18] for their AUSM⁺ scheme, and Romate [21] for his Roe scheme. Romate suggested a scheme switching strategy for solving this problem, where the original scheme is replaced with a stable, diffusive scheme near one-phase regions. Here we will follow a similar approach, using a strategy that has been previously applied with success [9]. We proceed as follows.

8.3.2. Modification of basic AUSMV and AUSMD splitting formulas.

We modify the parameters χ used in the splitting formulas (60) corresponding to the AUSMV and AUSMD schemes,

$$(85) \quad \chi_L = (1 - \phi_L) \frac{2(\rho/\alpha)_L}{(\rho/\alpha)_L + (\rho/\alpha)_R} + \phi_L$$

and

$$(86) \quad \chi_R = (1 - \phi_R) \frac{2(\rho/\alpha)_R}{(\rho/\alpha)_L + (\rho/\alpha)_R} + \phi_R,$$

for each phase. Here ϕ is the transition fix function

$$(87) \quad \phi = \phi(\alpha_g) = e^{-\Gamma_g \alpha_g} + e^{-\Gamma_1(1-\alpha_g)},$$

where Γ_k is a parameter controlling the diffusive effect of the transition fix. This fix ensures that we recover the more stable FVS/van Leer fluxes, as given by (56)–(59), in one-phase regions.

We observe that the transition to one-phase liquid flow (the denser phase) more easily induces instabilities than the transition to one-phase gas flow (the less dense phase). For the purposes of this paper, we choose the parameters

$$(88) \quad \Gamma_g = 50$$

and

$$(89) \quad \Gamma_1 = 500.$$

DEFINITION 8. *The modified AUSMD scheme as described by (85) and (86) will be denoted as the AUSMD* scheme. Similarly, the modified AUSMV scheme as described by (85) and (86) will be denoted as the AUSMV* scheme.*

8.3.3. WIMF-AUSMDV*. We consider convective fluxes which are a hybrid of those employed by AUSMD* and AUSMV* and are denoted as AUSMDV*. More precisely, the numerical convective fluxes $(\alpha\rho v)_{j+1/2}$ and $(\alpha\rho v^2)_{j+1/2}$ are given by the following expression:

$$(90) \quad \begin{aligned} (\alpha\rho v)_{j+1/2}^{\text{AUSMDV}^*} &= s(\alpha\rho v)_{j+1/2}^{\text{AUSMV}^*} + (1-s)(\alpha\rho v)_{j+1/2}^{\text{AUSMD}^*}, \\ (\alpha\rho v^2)_{j+1/2}^{\text{AUSMDV}^*} &= s(\alpha\rho v^2)_{j+1/2}^{\text{AUSMV}^*} + (1-s)(\alpha\rho v^2)_{j+1/2}^{\text{AUSMD}^*}. \end{aligned}$$

Here s is chosen as

$$(91) \quad s = \max(\phi_L, \phi_R),$$

where ϕ is the transition fix function given by (87). Note that this hybridization affects only the momentum convective fluxes since $(\alpha\rho v)_{j+1/2}^{\text{AUSMDV}^*} = (\alpha\rho v)_{j+1/2}^{\text{AUSMD}^*}$. The construction (90) ensures that AUSMDV* uses the accurate AUSMD* fluxes in two-phase regions and switches to the more stable AUSMV* fluxes in one-phase regions.

The WIMF-AUSMDV* scheme is now constructed straightforwardly by associating the fluxes F_k^A and G_k^A with the corresponding AUSMDV* fluxes as follows.

DEFINITION 9. We will use the term *WIMF-AUSMDV** to denote the numerical scheme given by (43)–(50), where $(F_k^D)_{j+1/2}^{n+1/2}$ is given by the pressure coherent component (55) whereas $(F_k^A)_{j+1/2}^n$ and $(G_k^A)_{j+1/2}^n$ are given by

$$(F_k^A)_{j+1/2}^n = (\rho\alpha v)_{k,j+1/2}^{\text{AUSMDV}^*,n}, \quad (G_k^A)_{j+1/2}^n = (\rho\alpha v^2)_{k,j+1/2}^{\text{AUSMDV}^*,n}.$$

Remark 11. It should be noted that we have no formal proof which guarantees that negative mass fractions will never be calculated by the proposed WIMF-AUSMDV* scheme. It does, however, work well on practical cases, while retaining the property of being fully consistent with the model formulation.

The idea of increasing the numerical dissipation near one-phase regions may be explored more systematically with the aim of obtaining more general relations that do not involve free parameters. Paillère, Corre, and Cascales [18] used a related approach, introducing a diffusion term depending on the pressure gradient to improve the performance of their AUSM+ scheme near one-phase liquid regions.

8.3.4. Numerical results. We now consider two different formulations of the two-fluid model:

- *Frictionless flow.* We assume that gravity is the only source term taken into account. In this case, the lack of friction terms causes the gas velocity to become large as the gas phase is disappearing. We note that for one-phase liquid flow we have $\alpha_l \gg \alpha_g$ and the volume fraction velocities (78) are dominated by this large gas velocity. Hence the weak CFL criterion (79) becomes very restrictive here. With this model we use the relatively low time step

$$(92) \quad \frac{\Delta x}{\Delta t} = 500 \text{ m/s}.$$

For stability of the FVS scheme, which AUSMDV* employs in the transition to single phase flow, we rescale the sound velocity c as described in the appendix, using

$$(93) \quad c = 750 \text{ m/s}$$

instead of the sound velocity determined from (12). This choice was based on the fact that we observed that the gas velocity could become as high as approximately 400 m/s. According to (120) in the appendix, we should then choose c such that $200 \leq c \leq 800$. We consistently have chosen c in the upper region.

- *Interfacial momentum exchange.* The low time step needed for the frictionless model is undesirable. In addition, the assumption of frictionless low is unphysical. In reality we expect the last remnants of the disappearing phase to be completely dissolved, and we expect $v_g \approx v_l$ near one-phase regions. To more realistically model this situation, we consider an interfacial momentum transfer model also used by Paillère, Corre, and Cascales [18]. For the gas momentum equation, we introduce the source term

$$(94) \quad M_g^D = C\alpha_g\alpha_l\rho_g(v_g - v_l),$$

where C is a positive constant. Likewise, the liquid momentum source term is given as

$$(95) \quad M_l^D = -M_g^D = -C\alpha_g\alpha_l\rho_g(v_g - v_l),$$

conserving total momentum. We write

$$(96) \quad C = C_0 \phi,$$

making the exchange term kick in more strongly near one-phase regions. Following [18], we set

$$(97) \quad C_0 = 50000 \text{ s}^{-1}.$$

To avoid stability problems related to stiffness in this term, we use a semi-implicit implementation as follows:

$$(98) \quad (M_g^D)_j^{n+1/2} = C_j^n (\alpha_g \alpha_l \rho_g)_j^n \left[\frac{(I_g)_j^{n+1}}{(m_g)_j^n} - \frac{(I_l)_j^{n+1}}{(m_l)_j^n} \right].$$

We found that we could now increase the time step to

$$(99) \quad \frac{\Delta x}{\Delta t} = 75 \text{ m/s},$$

consistent with the largest gas (volume fraction) velocities during the transient period. The sound velocity is rescaled as

$$(100) \quad c = 150 \text{ m/s}.$$

Again, this choice is based on the criterion (120), where we now can assume that the fluid velocity becomes zero in the transition to single-phase flow (due to the inclusion of the interfacial momentum transfer model). This gives us that c should be chosen in the interval $0 \leq c \leq 2\lambda = 2\Delta x/\Delta t$.

Results after $t = 0.6$ s are plotted in Figure 9, using a grid of 100 cells. The approximate analytical solutions (81) and (82) are used for reference. We note that good accordance with the expected analytical solutions is achieved. The most notable effect of the interfacial momentum exchange term is the reduction of the gas velocity in the one-phase liquid region.

Although the phases will be separated for $t < 1.0$ s, it takes some seconds before the excess momentum has been dissipated at the endpoints. Results for fully stationary conditions ($t = 5.0$ s) are plotted in Figure 10. We note that the frictionless model does not exactly yield the expected hydrostatic pressure distribution. This seems to be due to the strong velocity gradients at the separation point, and hydrostatic conditions are never fully reached. The inclusion of the interfacial friction term removes these gradients.

In Figure 11 the effect of grid refinement on the resolution of volume fraction is illustrated for the WIMF-AUSMDV* scheme with momentum exchange terms. The time step $\Delta x/\Delta t = 75$ m/s is used. The expected analytical solution is approached in a monotone way.

8.4. Oscillating manometer problem. Finally, we consider a problem introduced by Ransom [20] and investigated by Paillère, Corre, and Cascales [18] and Evje and Flåtten [9]. This problem tests the ability of numerical schemes to handle a change in the flow direction.

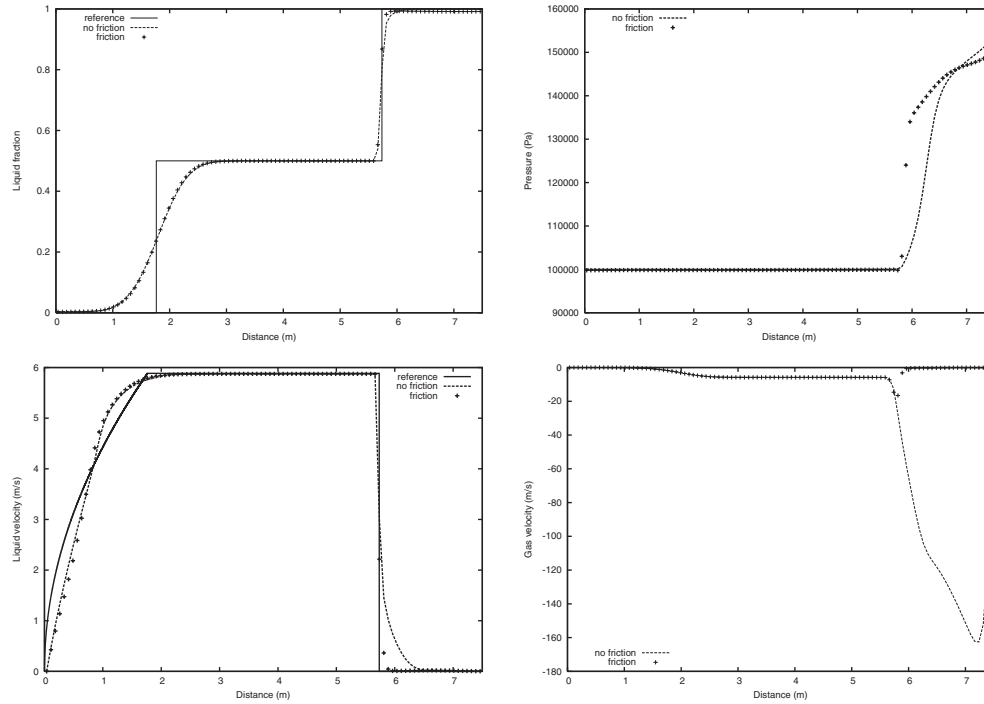


FIG. 9. Separation problem, $T = 0.6$ s, 100 grid cells. WIMF-AUSMDV* scheme with and without interfacial momentum exchange terms. Top left: liquid fraction. Top right: pressure. Bottom left: liquid velocity. Bottom right: gas velocity.

We consider a U-shaped tube of total length 20 m. The geometry of the tube is reflected in the x -component of the gravity field

$$(101) \quad g_x(x) = \begin{cases} g & \text{for } 0 \leq x \leq 5 \text{ m,} \\ g \cos\left(\frac{(x-5 \text{ m})\pi}{10 \text{ m}}\right) & \text{for } 5 \text{ m} < x \leq 15 \text{ m,} \\ -g & \text{for } 15 \text{ m} < x \leq 20 \text{ m.} \end{cases}$$

Initially we assume that the liquid fraction is given by

$$(102) \quad \alpha_1(x) = \begin{cases} 10^{-6} & \text{for } 0 \leq x \leq 5 \text{ m,} \\ 0.999 & \text{for } 5 \text{ m} < x \leq 15 \text{ m,} \\ 10^{-6} & \text{for } 15 \text{ m} < x \leq 20 \text{ m.} \end{cases}$$

The initial pressure is assumed to be equal to the hydrostatic pressure distribution. We assume that the gas velocity is uniformly $v_g = 0$, and the liquid velocity distribution is given by

$$(103) \quad v_1(x) = \begin{cases} 0 & \text{for } 0 \leq x \leq 5 \text{ m,} \\ V_0 & \text{for } 5 \text{ m} < x \leq 15 \text{ m,} \\ 0 & \text{for } 15 \text{ m} < x \leq 20 \text{ m,} \end{cases}$$

where $V_0 = 2.1$ m/s.

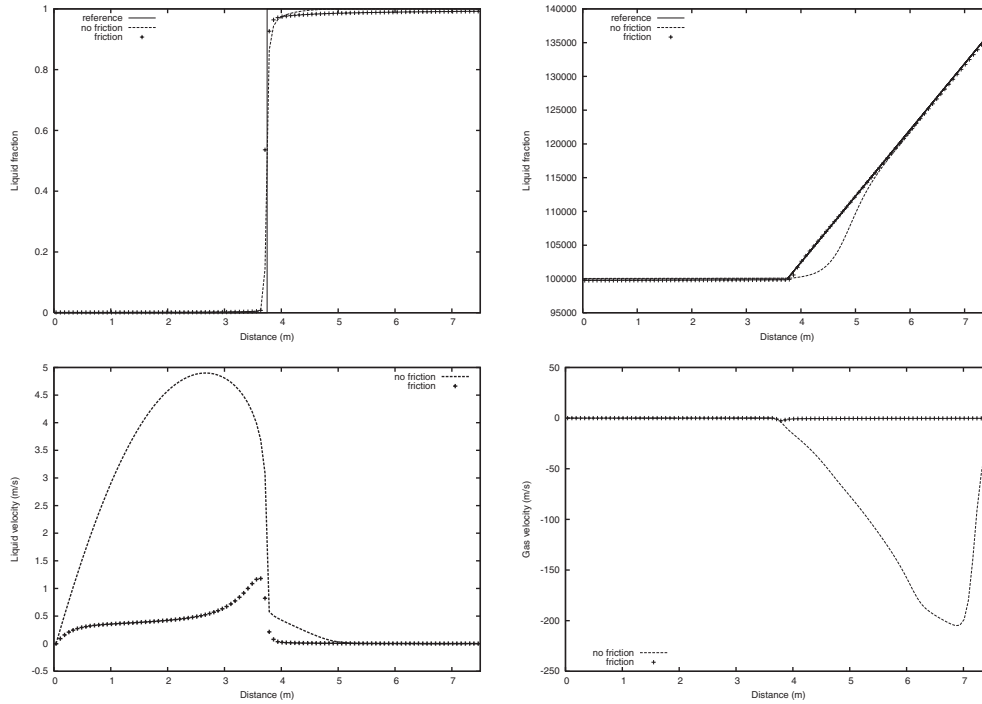


FIG. 10. Separation problem, $t = 5.0$ s, 100 grid cells. WIMF-AUSMDV* scheme with and without interfacial momentum exchange terms. Top left: liquid fraction. Top right: pressure. Bottom left: liquid velocity. Bottom right: gas velocity.

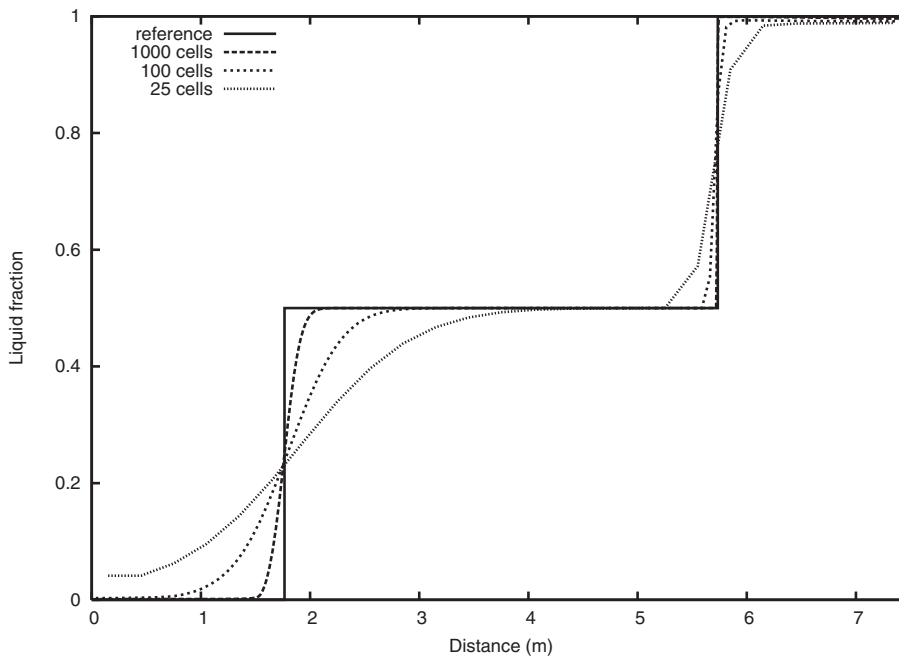


FIG. 11. Separation problem, $T = 0.6$ s. Convergence properties of the WIMF-AUSMDV* scheme with interfacial momentum exchange terms.

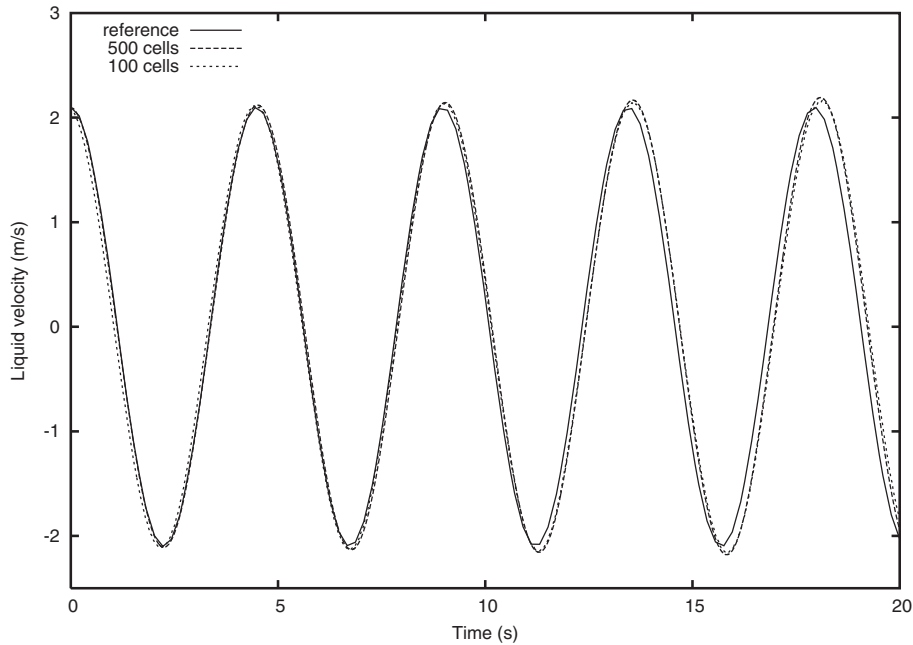


FIG. 12. *Oscillating manometer, WIMF-AUSMDV* scheme. Time development of the liquid velocity.*

Ransom [20] suggested treating the manometer as a closed loop. We will follow the approach of Paillère, Corre, and Cascales [18], assuming that both ends of the manometer are open to the atmosphere. We assume that the liquid column will move with uniform velocity under the influence of gravity, giving the following approximate analytical solution for the liquid velocity [18]

$$(104) \quad v_1(t) = V_0 \cos(\omega t),$$

where

$$(105) \quad \omega = \sqrt{\frac{2g}{L}},$$

where $L = 10$ m is the length of the liquid column.

To exploit the possibility of taking large time steps, we include the interfacial momentum exchange term as described in section 8.3.4. The sound velocity is rescaled to $c = 30$ m/s, which is consistent with (120), where we use that the fluid velocity is negligible in the transition to single-phase flow.

8.4.1. Numerical results. We consider the following grids:

- 100 cells—we use a time step corresponding to $\Delta x/\Delta t = 50$ m/s, and
- 500 cells—we use a time step corresponding to $\Delta x/\Delta t = 15$ m/s.

For the fine grid with 500 cells, the critical time step was found to be consistent with the weak CFL criterion (79). For the coarse grid consisting of 100 cells, a lower CFL number was needed to ensure stability. The evolution of the center cell liquid velocity is given in Figure 12. We note that the results for 100 and 500 cells are virtually identical, indicating that the resolution of the liquid velocity is not grid sensitive. We

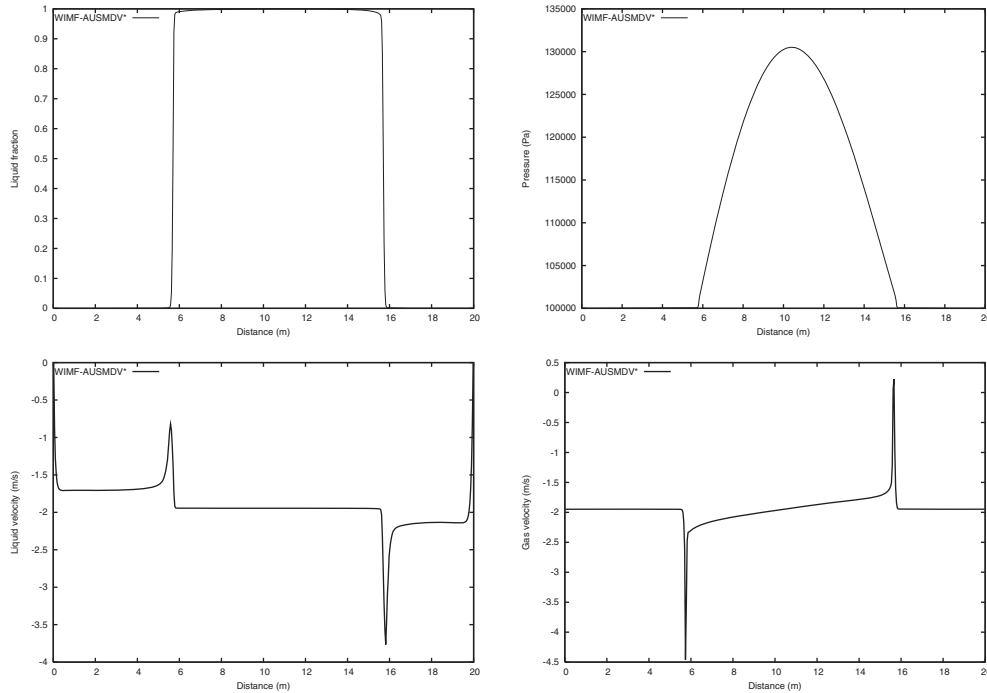


FIG. 13. *Oscillating manometer, $t = 20.0$ s, 500 grid cells. WIMF-AUSMDV* scheme. Top left: liquid fraction. Top right: pressure. Bottom left: liquid velocity. Bottom right: gas velocity*

observe a slight phase difference from the approximate analytical solution, as was also observed in [18, 9].

The distribution of all variables after $t = 20$ s is given in Figure 13 for the grid of 500 cells. We observe that the variables are approximated without any numerical oscillations. In particular there is little numerical diffusion for the volume fraction variable. The strong gradients in the velocities are a consequence of the sudden volume change at the transition points between the phases. We remark that the gas velocity was extrapolated at the boundaries, whereas the liquid velocity was forced to zero at the boundaries to avoid liquid mass leakage.

9. Summary. We have proposed a general framework for constructing weakly implicit methods for a two-fluid model. Particularly, we have constructed a weakly implicit numerical scheme, denoted as WIMF-AUSMD, that allows the CFL criterion for sonic waves to be violated. All the numerical experiments indicate that a weaker CFL criterion applies with relation to the slow-moving volume fraction waves.

The scheme is based on a mixture flux approach which properly combines diffusive and nondissipative fluxes to yield an accurate and robust resolution of sonic and volume fraction waves on nonstaggered grids. The sonic CFL criterion is violated by enforcing a coupling between the pressure wave component of the mixture flux, the cell center momenta, and the cell interface pressure. In particular all convective (mass and momentum) fluxes are treated in an explicit manner.

The numerical evidence indicates that the WIMF-AUSMD is highly robust and efficient and gives an accuracy potentially superior to the explicit Roe scheme on volume fraction waves. An added advantage of the WIMF-AUSMD scheme is that

it does not require a full eigenstructure decomposition of the Jacobi matrix for the system. However, the scheme is diffusive on pressure waves, especially for large time steps.

By increasing the numerical dissipation near one-phase regions, we have demonstrated that the framework allows for accurate, efficient, and robust solutions also for flow cases which locally involve the transition from one-phase to two-phase flow.

Appendix.

Rescaling the sound velocity. A problem with the original FVS scheme is that it can produce instabilities for large time steps if the discretization parameter $\lambda = \Delta x/\Delta t$ is chosen much smaller than the sound velocity. For an explicit scheme this will never be a problem as the CFL criterion limits the time steps we can take. For a semi-implicit method, however, we wish to use a value for λ that may be several orders of magnitude smaller than the physical sound velocity and the issue becomes of relevance. To describe the problem, we consider the mass conservation equation

$$(106) \quad \frac{\partial u}{\partial t} + \frac{\partial(uv)}{\partial x} = 0,$$

where $u = \rho_k \alpha_k$. We now consider the FVS scheme

$$(107) \quad (uv)_{j+1/2} = V^+(v_j, c)u_j + V^-(v_{j+1}, c)u_{j+1},$$

where we use the splitting formulas (56), assuming $v < c$,

$$(108) \quad V^\pm(v, c) = \pm \frac{1}{4c}(v \pm c)^2.$$

Total variation stability. We now take advantage of the following theorem due to Harten, as stated by Tadmor [24]

THEOREM 1. *Consider the scalar equation*

$$(109) \quad \frac{\partial u}{\partial t} + \frac{\partial f(u)}{\partial x} = 0$$

solved by the numerical scheme

$$(110) \quad \frac{u_j^{n+1} - u_j^n}{\Delta t} + \frac{1}{\Delta x} (F(u_j^n, u_{j+1}^n) - F(u_{j-1}^n, u_j^n)) = 0,$$

where the numerical flux $F(u_j^n, u_{j+1}^n)$ is written in viscous form

$$(111) \quad F_{j+1/2} = F(u_j^n, u_{j+1}^n) = \frac{1}{2} (f(u_j^n) + f(u_{j+1}^n)) - \frac{1}{2} \frac{\Delta x}{\Delta t} Q_{j+1/2}^n (u_{j+1}^n - u_j^n).$$

The scheme (110) is total variation nonincreasing provided its numerical viscosity coefficient $Q_{j+1/2}^n = Q(u_j^n, u_{j+1}^n)$ satisfies

$$(112) \quad \frac{\Delta t}{\Delta x} \left| \frac{f(u_{j+1}^n) - f(u_j^n)}{u_{j+1}^n - u_j^n} \right| \leq Q_{j+1/2}^n \leq 1.$$

For the scheme (107) using the splitting formulas (108) we obtain the numerical viscosity coefficient

$$(113) \quad Q_{j+1/2}^n = \frac{\Delta t}{\Delta x} \frac{v^2 + c^2}{2c}.$$

Using this and assuming uniform velocity we can write the requirement (112) as

$$(114) \quad \frac{\Delta t}{\Delta x} v \leq \frac{\Delta t}{\Delta x} \frac{v^2 + c^2}{2c} \leq 1,$$

which yields the following lemma.

LEMMA 3. *Let the mass equation (106) be solved using the numerical fluxes given by (107) and (108). Then the resulting scheme is total variation nonincreasing if*

$$(115) \quad \frac{\Delta x}{\Delta t} \geq \frac{v^2 + c^2}{2c}$$

and

$$(116) \quad c > 0.$$

The criterion (115) attains its minimum value for $v = c$, for which we obtain

$$(117) \quad \frac{\Delta x}{\Delta t} \geq v,$$

which is the standard CFL criterion.

To further investigate how c should be chosen, we now assume that

$$(118) \quad \lambda = \frac{\Delta x}{\Delta t}$$

is known and investigate which criteria govern the possible choices for c . From (115) we obtain

$$(119) \quad c^2 - 2c\lambda + v^2 \leq 0.$$

Solving this equation we obtain the following corollary.

COROLLARY 1. *Let the linear advection equation (106) be solved using the numerical fluxes given by (107) and (108). Assume the time step $\lambda = \Delta x/\Delta t$ is known. Then the resulting scheme is total variation nonincreasing if the sound velocity c satisfies*

$$(120) \quad \lambda - \sqrt{\lambda^2 - v^2} \leq c \leq \lambda + \sqrt{\lambda^2 - v^2}.$$

This result is confirmed by numerical experiments and illustrates that if $c \gg \lambda$ the FVS scheme is unstable. We hence propose to rescale the sound velocity used in the flux splitting schemes such that the requirement (120) is satisfied also for large time steps. We stress that this step is necessary to achieve stability on the *advective* effects for the FVS scheme. Stability of the *sonic* waves is an independent problem that we wish to achieve through taking advantage of the implicit pressure-momentum coupling together with the decomposition of F_k into F_k^D and F_k^A .

Acknowledgments. The authors thank the reviewers for carefully reading through the manuscript and making several useful comments.

REFERENCES

- [1] R. ABGRALL, *How to prevent pressure oscillations in multicomponent flow calculations*, J. Comput. Phys., 125 (1996), pp. 150–160.
- [2] F. BARRE AND M. BERNARD, *The cathare code strategy and assessment*, Nuclear Engrg. Des., 124 (1990), pp. 257–284.
- [3] K. H. BENDIKSEN, D. MALNES, R. MOE, AND S. NULAND, *The dynamic two-fluid model OLGA: Theory and application*, SPE Prod. Eng., 6 (1991), pp. 171–180.
- [4] F. COQUEL, K. EL AMINE, E. GODLEWSKI, B. PERTHAME, AND P. RASCLE, *A numerical method using upwind schemes for the resolution of two-phase flows*, J. Comput. Phys., 136 (1997), pp. 272–288.
- [5] J. CORTES, A. DEBUSSCHE, AND I. TOUMI, *A density perturbation method to study the eigenstructure of two-phase flow equation systems*, J. Comput. Phys., 147 (1998), pp. 463–484.
- [6] J. R. EDWARDS, R. K. FRANKLIN, AND M.-S. LIOU, *Low-diffusion flux-splitting methods for real fluid flows with phase transition*, AIAA J., 38 (2000), pp. 1624–1633.
- [7] S. EVJE AND K. K. FJELDE, *Hybrid flux-splitting schemes for a two-phase flow model*, J. Comput. Phys., 175 (2002), pp. 674–701.
- [8] S. EVJE AND K. K. FJELDE, *On a rough AUSM scheme for a one-dimensional two-phase flow model*, Comput. & Fluids, 32 (2003), pp. 1497–1530.
- [9] S. EVJE AND T. FLÅTTEN, *Hybrid flux-splitting schemes for a common two-fluid model*, J. Comput. Phys., 192 (2003), pp. 175–210.
- [10] I. FAILLE AND E. HEINTZÉ, *A rough finite volume scheme for modeling two-phase flow in a pipeline*, Comput. & Fluids, 28 (1999), pp. 213–241.
- [11] K.-K. FJELDE AND K. H. KARLSEN, *High-resolution hybrid primitive-conservative upwind schemes for the drift flux model*, Comput. & Fluids, 31 (2002), pp. 335–367.
- [12] M. LARSEN, E. HUSTVEDT, P. HEDNE, AND T. STRAUME, *Petra: A novel computer code for simulation of slug flow*, in SPE Annual Technical Conference and Exhibition, Society of Petroleum Engineers, 1997.
- [13] M.-S. LIOU, *A sequel to AUSM: AUSM(+)*, J. Comput. Phys., 129 (1996), pp. 364–382.
- [14] J. M. MASELLA, Q. H. TRAN, D. FERRE, AND C. PAUCHON, *Transient simulation of two-phase flow in pipes*, Int. J. Multiphase Flow, 24 (1998), pp. 739–755.
- [15] J. M. MASELLA, I. FAILLE, AND T. GALLOUET, *On an approximate Godunov scheme*, Int. J. Comput. Fluid. Dyn., 12 (1999), pp. 133–149.
- [16] Y. Y. NIU, *Simple conservative flux splitting for multi-component flow calculations*, Num. Heat Trans., 38 (2000), pp. 203–222.
- [17] Y.-Y. NIU, *Advection upwinding splitting method to solve a compressible two-fluid model*, Internat. J. Numer. Methods Fluids, 36 (2001), pp. 351–371.
- [18] H. PAILLÈRE, C. CORRE, AND J. R. G CASCALES, *On the extension of the AUSM+ scheme to compressible two-fluid models*, Comput. & Fluids, 32 (2003), pp. 891–916.
- [19] S. V. PATANKAR, *Numerical Heat Transfer and Fluid Flow*, Taylor & Francis, Philadelphia, 1980.
- [20] V. H. RANSOM, *Numerical benchmark tests*, Multiphase Sci. Tech., 3 (1987), pp. 465–473.
- [21] J. E. ROMATE, *An approximate Riemann solver for a two-phase flow model with numerically given slip relation*, Comput. & Fluids, 27 (1998), pp. 455–477.
- [22] R. SAUREL AND R. ABGRALL, *A multiphase Godunov method for compressible multifluid and multiphase flows*, J. Comput. Phys., 150 (1999), pp. 425–467.
- [23] R. SAUREL AND R. ABGRALL, *A simple method for compressible multifluid flows*, SIAM J. Sci. Comput., 21 (1999), pp. 1115–1145.
- [24] E. TADMOR, *Numerical viscosity and the entropy condition for conservative difference schemes*, Math. Comp., 43 (1984), pp. 369–381.
- [25] I. TOUMI, *An upwind numerical method for two-fluid two-phase flow models*, Nuclear Sci. Engrg., 123 (1996), pp. 147–168.
- [26] I. TOUMI AND A. KUMBARO, *An approximate linearized riemann solver for a two-fluid model*, J. Comput. Phys., 124 (1996), pp. 286–300.
- [27] J. A. TRAPP AND R. A. RIEMKE, *A nearly-implicit hydrodynamic numerical scheme for two-phase flows*, J. Comput. Phys., 66 (1986), pp. 62–82.
- [28] Y. WADA AND M.-S. LIOU, *An accurate and robust flux splitting scheme for shock and contact discontinuities*, SIAM J. Sci. Comput., 18 (1997), pp. 633–657.